Ultrasonics Sonochemistry 115 (2025) 107291

Contents lists available at ScienceDirect

Ultrasonics Sonochemistry

journal homepage: www.elsevier.com/locate/ultson

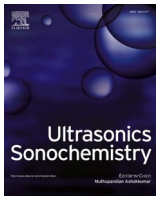

The impact of radicals on physicochemical properties of waste activated sludge during hydrodynamic cavitation treatment

Marko Blagojević [a], Mojca Zupanc [b], Jurij Gostiša [b], Blaž Stres [a,c,d,e], Alenka Šmid [f], Matevž Dular [b], Lidija Slemenik Perše [b], Urška Gradišar Centa [b], Benjamin Bizjan [a,b], Gašper Rak [b], Uroš Novak [e], Blaž Likozar [e], Sabina Kolbl Repinc [a,e,*]

[a] Faculty of Civil and Geodetic Engineering, University of Ljubljana, Jamova cesta 2, 1000 Ljubljana, Slovenia
[b] Faculty of Mechanical Engineering, University of Ljubljana, Aškerčeva cesta 6, 1000 Ljubljana, Slovenia
[c] Biotechnical Faculty, University of Ljubljana, Jamnikarjeva ulica 101, 1000 Ljubljana, Slovenia
[d] Jozef Stefan Institute, Jamova cesta 39, 1000 Ljubljana, Slovenia
[e] National Institute of Chemistry, Hajdrihova ulica 19, 1000 Ljubljana, Slovenia
[f] Faculty of Pharmacy, University of Ljubljana, Ljubljana, Slovenia

ARTICLE INFO

Keywords:
Waste-activated sludge
Hydrodynamic cavitation
Pinned disc
Radicals
UV–Vis
Rheology
Methane

ABSTRACT

In this study, laboratory-scale Pinned Disc Rotary Generator of Hydrodynamic Cavitation was used to treat waste-activated sludge with a Total Solids concentration of 0.7 %. Five different rotor–stator arrangements were tested, focusing on waste-activated sludge physicochemical and rheological parameters of industrial relevance: general chemical analysis, rheometry, dewaterability, interfacial tension, UV–Vis and FTIR spectroscopy. Radical formation in all five arrangements was confirmed using salicylic acid dosimetry before sample testing. Three of the arrangements generated twice the radical concentration of the other two and achieved a disintegration degree three times higher (17 % compared to 5 %). Capillary Suction Time tests demonstrated a 14-fold reduction in filterability across all arrangements, accompanied by an increase in interfacial tension exceeding 10 %. Statistically significant changes in the UV–Vis spectra indicated alterations in dissolved organic matter humification, aromaticity, and molecular size of colorimetric dissolved organic matter, DNA, and RNA. FTIR analysis revealed characteristic peaks at 1537 cm^{-1} and 1648 cm^{-1}, signifying microbial cell wall damage. Rheological analysis showed a reduction in apparent viscosity within the low shear stress zone ($\tau < 5$ Pa) and a shift in the yield stress point to lower shear stresses ($\tau < 0.14$ Pa compared to $\tau = 0.17$ Pa for the untreated samples). Pearson's correlation test revealed strong, statistically significant correlations between cell wall damage (as identified by FTIR) and hydrodynamic conditions in the reactor, while the correlation with radical formation was not statistically significant. This suggests that hydrodynamic forces were the primary drivers of cell wall damage, with potential synergetic effects from radicals.

1. Introduction

Water resources face escalating strain and depletion due to modernization, population increase and emergence of new pollutants. To achieve robust sustainable development, wastewater must be effectively treated, with biological wastewater treatment plants (WWTP) serving as the cornerstone. These treatment plants rely on complex microbial communities, including bacteria, archaea, protozoa, fungi, and other microorganisms, collectively known as Activated Sludge (AS), which play a pivotal role in eliminating organic matter and degrading diverse pollutants [1].

A significant byproduct of the AS process is the generation of substantial quantities of waste-activated sludge (WAS) [2]. One of the most widely used techniques for stabilizing and reducing WAS volume is anaerobic digestion (AD). During AD, anaerobic microorganisms degrade organic matter while simultaneously producing biomethane, CO_2 and other trace gases in the absence of oxygen, a renewable energy source, which can be harnessed to generate electricity, covering a portion of the power demand for WWTP operations. Among various pretreatment methods aimed at increasing biogas yield, hydrodynamic

* Corresponding author at: Faculty of Civil and Geodetic Engineering, University of Ljubljana, Jamova cesta 2, 1000 Ljubljana, Slovenia.
E-mail address: sabina.kolbl-repinc@fgg.uni-lj.si (S. Kolbl Repinc).

https://doi.org/10.1016/j.ultsonch.2025.107291
Received 25 November 2024; Received in revised form 19 February 2025; Accepted 24 February 2025
Available online 24 February 2025

cavitation (HC) has emerged as particularly promising. Several studies have highlighted the positive effects of HC treatment on WAS, including reduced digester volumes and hydraulic retention time, accelerated decomposition of volatile solids [3], improved settleability [4] and enhanced biogas production [5–10].

HC treatment of WAS demonstrated its effectiveness in damaging and breaking microbial cell walls and organic materials. During HC, the collapse of cavitation bubbles generates extreme local conditions, with temperatures reaching up to several thousand degrees Celsius and pressures up to several hundred atmospheres. These conditions cause the thermal decomposition of water molecules ($H_2O \rightarrow {}^{\bullet}H + {}^{\bullet}OH$), producing highly reactive hydroxyl radicals ($^{\bullet}OH$) and hydrogen radicals ($^{\bullet}H$) [11]. These can be measured through coumarin dosimetry [12], the chemiluminescence method [13] and salicylic acid (SA) dosimetry [14].

Extracellular polymeric substances (EPS), which comprise approximately half of the organic matter in WAS, are composed of high-molecular-weight biomolecules, including proteins, polysaccharides, humic substances, nucleic acids, and lipids [15]. These biomolecules form a matrix that holds microbial cells together, influencing the formation and stability of flocs. Hydroxyl radicals, generated through HC, can further form hydrogen peroxide (H_2O_2) and oxidize functional groups within EPS. This process results in the degradation and destruction of the sludge matrix [15,16], enhancing cell membrane permeability. Consequently, there is a partial release of biofilm matrices, EPS, intracellular matter, and DNA into the liquid phase, making these components more accessible for hydrolysis, the rate-limiting step in the AD process [17].

While the impact of cavitation on sludge rheology has been extensively studied in the past, notably through acoustic cavitation [18–21] and Ferro-sonication [22], these methods differ in their mechanisms and effects. Acoustic cavitation involves the use of high-frequency ultrasound to induce the formation and collapse of microbubbles, resulting in intense mechanical shear forces and chemical effects, such as the generation of reactive oxygen species. Ferro-sonication on the other hand, combines ultrasound with the Fenton oxidation process, where iron-based catalysts (e.g., Fe^{2+} or Fe^{3+}) react with H_2O_2 to generate $^{\bullet}OH$, further enhancing the breakdown of organic matter. In comparison to these methods, rheological characteristics of HC-treated sludge [8,9,23] remain less explored, particularly beyond classical flow curves (for example lack of amplitude sweep tests). Consequently, the examination of complex rheological properties remains an area warranting further investigation. Our preliminary study [24] has shown that HC treatment affects viscosity under low shear stress conditions in waste sludge with 3.7 % total solids (TS) due to fragmentation and physicochemical changes. Therefore, one of the objectives of this study was to extend the investigation to sludge with lower TS content and measure complex rheological parameters, such as the storage (G') and loss modulus (G'').

With that in mind, this study aims to measure $^{\bullet}OH$ production and evaluate their contribution to the treatment of WAS. By incorporating SA dosimetry [14], we evaluated radical production in the Pinned Disc Rotary Generator of Hydrodynamic Cavitation (PD-RGHC) across different rotor–stator configurations and convoluted their impact on the physicochemical changes in WAS. Using the same experimental setup as in previous research [24] utilizing a sample with defined chemical properties, we seek to provide a deeper understanding of the effects of HC treatment on physicochemical properties and the role of radicals in these HC processes.

This work builds upon past theories on the interaction of HC on water and organic materials [8,9,23–26]. The hypothesis of this study is that radical production and hydrodynamic forces during HC treatment significantly influence the physicochemical properties of WAS. Second, we hypothesize that forces during HC treatment specifically modify dissolved organic matter composition as measured through FTIR and UV–Vis spectroscopy, influences rheological behavior (Amplitude sweep test), and cell wall integrity, as determined by FTIR.

This study aims to elucidate the interplay between radicals and hydrodynamic conditions in the PD-RGHC setup, previously explored [8,24,27,28], focusing on their relative contributions to WAS disintegration and structural modifications. These structural changes, driven by the combined effects of hydrodynamic forces and radicals at both macro and micro scales, are expected to have a profound impact on the rheological properties of WAS, which are crucial for pumping, transport, and dewatering processes at the industrial level, as suggested before [18,21,24,29].

2. Materials and methods

2.1. Cavitation device

The laboratory-scale PD-RGHC, developed by Gostiša et al. [28], was used in this study, Fig. 1. The five rotor–stator arrangements selected for WAS treatment were identified as the most aggressive by Gostiša et al. [27,28] and had shown promising results in preliminary tests on WAS with 3.7 % TS [24]. Recent research by Zupanc et al. [8] further demonstrated the effectiveness of pinned disc configuration in enhancing biomethane production, driving ongoing investigations.

The PD-RGHC features a rotor and stator disc with equidistant cavitation generation units (CGUs), which in this study were cylindrical pins or prism elements. Cavitation is induced by pressure drops and shear forces as the rotor CGUs pass the stator CGUs. In this study, we evaluated five rotor–stator arrangements previously tested in our earlier research [24]. Throughout the manuscript, these rotor–stator arrangements are referred to by their configuration IDs, as shown in Fig. 2. For further details on the rotor–stator geometry, see Gostiša et al. [28].

In all cases, 4 L of WAS was treated for 30 consecutive cavitation passes; $Np = Q \bullet t/V$, where Q is the flow rate, t cavitation time and V volume of treated sludge. HC tests were conducted at room temperature (23 °C), 46 % relative humidity, and ambient pressure (985 mbar).

2.2. Salicylic acid dosimetry

The influence of different rotor–stator configurations on the formation of $^{\bullet}OH$ was investigated using salicylic acid (SA) dosimetry. During HC treatment, the $^{\bullet}OH$ generated react with SA to produce the following hydroxylated products: 2,3-dihydroxybenzoic acid (2,3-DHBA); 2,5-dihydroxybenzoic acid (2,5-DHBA); and 1,2-dihydroxybenzene (1,2-DHB). These products serve as markers for $^{\bullet}OH$ generation and allow the comparison of radical formation during the investigated HC treatments. An analytical method with HPLC coupled to a UV–Vis detector was used to determine the concentration of these SA products. The standards used for the analysis were of analytical grade and were purchased from Sigma-Aldrich (SA $\geq$ 99 %, 2,3-DHBA $\geq$ 99 %, 2,5-DHBA $\geq$ 98 % and 1,2-DHB $\geq$ 99 %). The analysis of SA products and the validation of the analytical method are described in detail in Zupanc et al. [14]. The SA stock solutions with a concentration of 300 mg/L were prepared in distilled water on the day of the experiments. Before the HC experiments, 4 L of the SA solution was acidified with 1 M HCl, purchased from Honeywell Fluka to a pH of around 2.5 (below the pKa of SA, which is 2.97). For HPLC analysis, 1 mL of the sample was withdrawn after 0, 25, 75 and 150 cavitation passes. The temperature was kept below 30 °C during the experiments. Chromatograms for pure SA and standard solutions with the three analytes (1,2-DHB; 2,3-DHBA and 2,3-DHBA) are provided in Suppl. Material 1, Section 4, Fig. 4 and 4.2S. Analyte quantification was performed at the following wavelengths: 1,2-DHB at 278 nm; 2,3-DHBA at 247 nm; and 2,5-DHBA at 320 nm. The corresponding calibration curves are available in Supplementary Material, Section 4 Fig. 4.3S.

2.3. WAS sample origin

The WAS sample was obtained from the Ljubljana Central Wastewater Treatment Plant, which processes around 82.200 m^3/day of dry

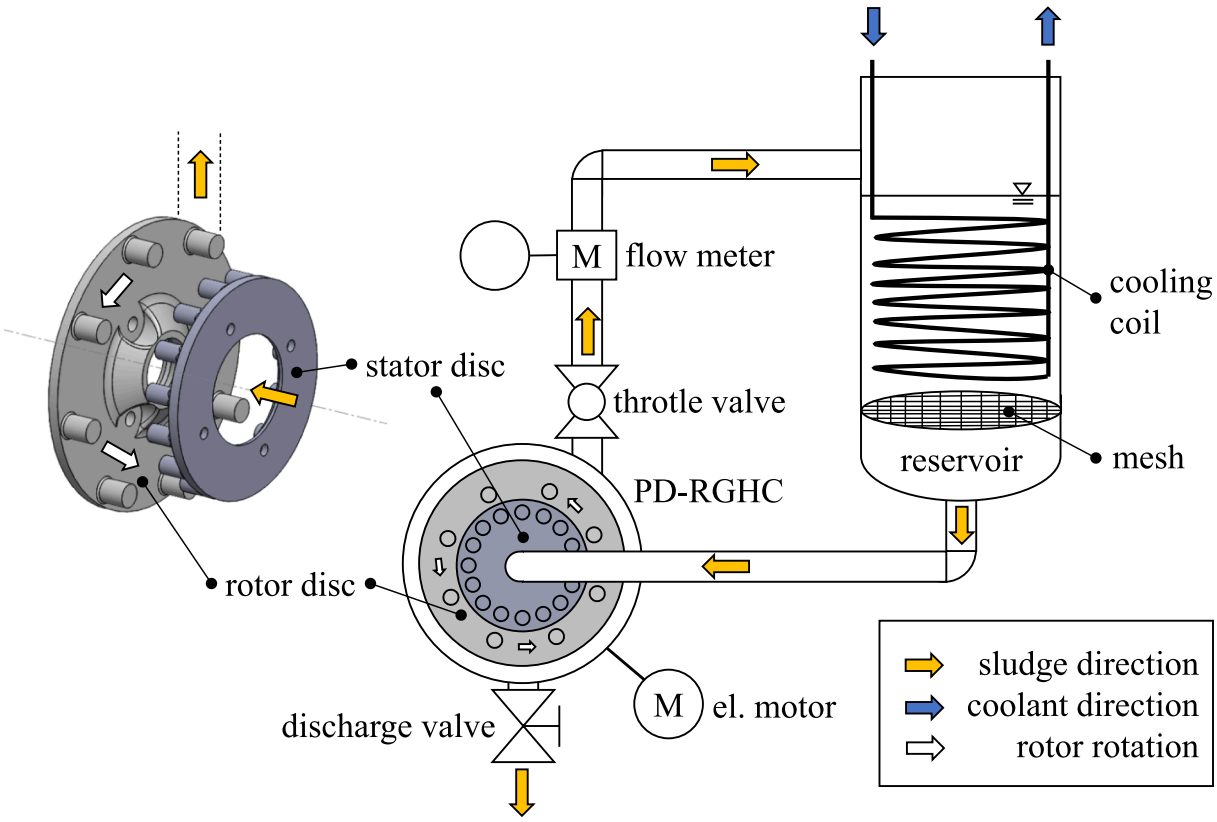

Fig. 1. Schematic representation of Pinned Disc Rotary Generator of Hydrodynamic Cavitation (PD-RGHC) measuring line, adapted with permission from reference [24]. 2024, Elsevier.

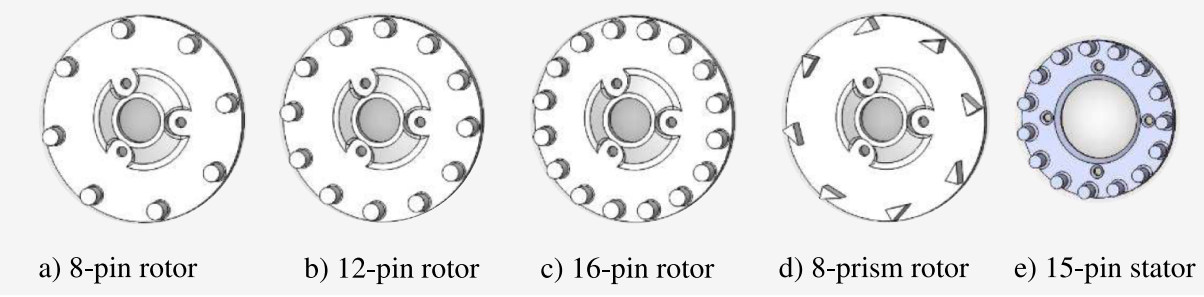

Fig. 2. Rotor-stator arrangements employed in the study and their characteristics.

flow, a peak flow of 103.500 m^3/day and a peak flow of 157.000 m^3/day of wastewater daily. The plant, designed for 360,000 population equivalents (PE), handles wastewater comprising 62 % municipal, 21 % stormwater, 11 % industrial, and 6 % foreign water [30].

After treatment, sludge undergoes AD in two mesophilic digesters (20 m diameter, 23 m height, 14,600 m^3 total volume) with a retention time exceeding 25 days. This process produces about 5,100 Nm^3/day of biogas, with 60 % to 64 % biomethane content [30].

For the experiment, 60 L of WAS were collected (before the polymer addition step utilized at the WWTP) to preserve its original composition. The sample was refrigerated at 7 °C overnight to prevent fermentation and microbial degradation and was homogenized manually for uniformity before conducting the experiments as described before [24].

2.4. WAS physicochemical analysis

Total solids (TS), volatile solids (VS), and sludge volume index (SVI) were measured following the APHA guidelines [31]. For additional details, refer to Suppl. Material 1, Section 1.

Temperature, pH, electric conductivity (EC), and oxidation–reduction potential (ORP), were measured with an HQ40D portable Multimeter and Intelligent HQD IntelliCAL Probe (Hach), calibrated per the manufacturer's guidelines. These parameters were assessed before, during (with the probe immersed in the reservoir), and after HC [8,17,24].

Total chemical oxygen demand (TCOD) and soluble COD (sCOD) were determined with appropriate cuvette tests (Hach-Lange, Germany). Total phosphorus (TP), Orthophosphate (PO_4-P) and soluble ammonium (sNH_4) were measured with test kits according to the manufacturer's instructions (Hach-Lange, Germany). For soluble component preparation, the supernatant was obtained by centrifugation at 15,000 RPM (21.630g) for 10 min and subsequent filtration through a 0.45 μm pore size filter (Chromafil Xtra CA-45/25). Cuvettes were analyzed using a DR 2800 spectrophotometer (Hach-Lange, Germany) [8,17,24,32].

WAS filterability, expressed as Capillary Suction Time (CST) in

seconds, was assessed using a type 304 M CST apparatus (Tritonel). Lower CST values indicate better dewatering performance. The sludge sample was mixed thoroughly before CST was measured with an 18 mm diameter stainless steel funnel. Measurements were taken immediately after cavitation, performed in triplicate, and averaged [24].

Particle size distribution of WAS was measured using laser diffraction technology with Particle Size Analyzer Analysette 22 – Wet Dispersion Unit (Fritsch, Germany), as described before [8,17,24].

The physicochemical properties of the untreated WAS sample are detailed in Table 1.

2.5. Interfacial tension

The interfacial tension (IFT) or surface tension of WAS was assessed using a K20 EasyDyne tensiometer from Krüss GmbH (Hamburg, Germany) at 25 °C. The Wilhelmy plate method was used with a 19 mm platinum plate and a wetted length of 40.20 mm. Measurements were taken in triplicate within 24 h post-cavitation, with samples stored in the dark at 7 °C [24].

2.6. Ultraviolet–visible spectroscopy (UV–Vis)

First, samples were centrifuged at 3200 g for 10 min, and the supernatant was filtered through a 0.45 µm pore size filter. Then, 200 µl of each sample was pipetted onto a microtiter plate. Samples were measured with a UV–Vis spectrophotometer across the 200–900 nm wavelength range in 1 nm steps, using deionized water as a negative control. Measurements were made in triplicate and averaged.

For the characterization of dissolved organic matter (DOM), we employed the spectrophotometric parameterization approach by Helms et al. [8,17,33]. Colorimetric DOM (CDOM) was characterized by calculating molecular weight indices and slope ratios from the absorption spectra: A254 (organic compounds), SumA250-A450 (sum of absorbance from A250 to A450; CDOM concentration), E2:E3 (ratio A250/A365; relative size of DOM molecules), E4:E6 (ratio A465/A665; humification and aromaticity), and slope ratio (SR) of the regions 275–295 nm and 350–400 nm (molecular weight and CDOM degradation) [8,17].

Next, nucleic acids were characterized using characteristic wavelengths: A230 (carbohydrates and aromaticity), A260 (DNA, RNA), A280 (proteins) and A320 (colorimetric DOC). DNA purity indices, DNA1 (A260/A230), DNA2 (A260/A280) and DNA3 (A260/A320) were calculated to determine the contribution of non-DNA compounds to the changes observed as described before [17].

2.7. Fourier-transform infrared spectroscopy (FTIR)

For the FTIR analysis, soluble fraction was analyzed using ATR-FTIR Omega 2 spectrometer (Perkin Elmer, USA) with wavenumbers ranging from 400 cm^{-1} to 4000 cm^{-1} and a resolution of 1 cm^{-1} as described before [34].

Table 1
Physicochemical properties of WAS sample. For parameter abbreviations please see Materials and methods (2.4. WAS physicochemical analysis). All measurements were performed in triplicate and are reported as mean ± standard deviation.

parameter	unit	value ± sd
TS	%	0.67 ± 0.01
VS	% of TS	68.1 ± 0.2
SVI	ml/g	123 ± 2
pH	–	6.97 ± 0.02
EC	µS/cm	577 ± 1
ORP	mV	38.5 ± 0.7
TCOD	mg/l	10130 ± 365
sCOD	mg/l	90 ± 1
sNH_4-N	mg/l	4.6 ± 0.4
sTP	mg/l	185.4 ± 1.4
PO_4-P	mg/l	42.7 ± 1.4
CST	s	23.9 ± 0.9

2.8. Rheological analysis

Flow and dynamic measurements were performed using an Anton Paar MCR302 rheometer. The analyses were conducted in a thermal chamber maintained at a constant temperature of 25 °C. A parallel plate measuring system was utilized, as it offers lower sensitivity to settling [35], featuring a PP25-S (S-Sandblasted) measuring body for the upper plate and an INSET/pp25/SS/S D:25 mm, HETD 400 for the lower plate, with a set gap of 1 mm.

Flow measurements were carried out in the shear stress range from 0.01–10 Pa at a constant frequency of 1 Hz. In the amplitude sweep test, the upper limit of the linear viscoelastic (LVE) range was determined within the shear strain ($\gamma = s/h$, where s is the deflection path and h shear gap) range from 0.01–100 % at the same frequency of 1 Hz. During the test, the applied stress was linearly increased over the entire duration of the test, 6.2 min. For detailed information on storage modulus (G') and loss modulus (G''), refer to Suppl. Material 1, Section 2.

2.9. Biochemical methane potential test (BMP)

To determine the BMP of treated WAS, a test was conducted using the AMPTS II system (BPC, Sweeden). The experiment utilized 0.5 L reactors in a temperature-controlled water bath at 38 °C. Each reactor was loaded with 300 mL of digestate from the Central WWTP Ljubljana as the inoculum and 70 mL of WAS as the substrate. Mixing was achieved with electric motors cycling 5 min on and 10 min off. CO_2 in the biogas was captured using 100 mL glass bottles, with 80 ml 3 M NaOH (Sigma-Aldrich, Germany) [8,17,24]. Physicochemical parameters of the inoculum are available in Suppl. Material 1, Section 3.

2.10. Statistical analysis

The experimental results were analyzed using PAST software version 4.12b [36], employing a combination of univariate and multivariate statistical methods to ensure comprehensive data evaluation. The univariate analysis utilized the Kruskal–Wallis test to determine statistically significant differences ($p < 0.05$) among groups on an individual parameter basis, followed by Dunn's post hoc test to identify specific pairwise differences. For multivariate analysis, a one-way PERMANOVA was conducted to assess statistically significant differences ($p < 0.05$) among groups, based on both, selected and overall data compositions. To visualize these multivariate relationships, non-metric multidimensional scaling (nmMDS) was employed. Furthermore, Pearson's (r) and Spearman's correlation tests were employed to gain insight into the relationships and correlations among the investigated parameters. Additional details regarding the statistical methods can be found in the PAST user manual [37].

3. Results and discussion

3.1. Determination of salicylic acid products for assessing radical formation

The concentration of SA products is an important indicator for evaluating the formation of $^{\bullet}OH$ during HC treatment. These radicals are highly reactive and play a critical role in degrading organic matter and enhancing sludge treatment processes. Three SA products (2,3-dihydroxybenzoic acid (2,3-DHBA), 2,5-dihydroxybenzoic acid (2,5-DHBA) and 1,2-dihydroxybenzene (1,2-DHB)) were measured for each rotor–stator configuration at the following *Np*: 25, 50, 75, 100, and 150 (results available in Suppl. Material 1, Section 5, Fig. 4.2S). For each configuration, as *Np* increased, so did the concentration of all three SA

products, indicating a correlation between cavitation treatment time and product formation. 2,3-DHBA was found to be the predominant product among the three, as also shown and discussed in detail in our previous study investigating the effects of the Venturi HC design [14]. It is very difficult to compare the results when different cavitation types and devices are used, especially due to the different energy inputs. However, comparing the results obtained during the study with those of the Venturi design, similar concentration ranges of SA products were achieved after 75 cavitation passes (after approximately 10 min, which is comparable to the 15-minute treatment in the Venturi HC) for the 8pin and 12pin designs.

From the measured SA products (2,3-DHBA, 2,5-DHBA and 1,2-DHB) the total SA product concentration (denoted as SA_{yield}) was calculated for each rotor–stator configuration. Trendlines were then fitted to analyze SA product generation for the five configurations in respect to *Np*, Fig. 3 (details in Suppl. Material 1, Section 5). Linear trendlines provided the best fit for configurations with pinned rotor discs (8pin, 12pin, 16pin and 8pin-NS) with ($R^2 > 0.99$), while the 8prism configuration was best approximated with a second-order polynomial ($R^2 > 0.99$). The 8pin, 12pin and 8prism regimes performed similarly in terms of SA production up to 50 passes. However, for longer treatment times, the 8pin and 12pin designs outperformed the 8prism design, indicating that the concentrations of SA products formed vary between different geometries. The lowest concentrations were measured for the 16pin and 8pin-NS geometries. The amount of measured SA products is well supported by the reported effective pressure values, as well as the average area and standard deviation of the cavitation cloud, which were all higher for the 8pin, 12pin, and 8prism rotor geometries [28].

3.2. Physicochemical changes in waste-activated sludge

The physicochemical properties of WAS are critical for understanding the effects of HC treatment and optimizing its application in sludge management processes. Temperature, pH, EC, ORP, and the solubility of chemical components are essential indicators that reflect the extent of structural and chemical alterations induced by HC.

The initial temperature of WAS sample before treatment was 16 ± 1 °C. Following the treatment process, temperature elevation values were recorded as follows: an increase of 7.2 ± 0.4 °C for the 8pin configuration, 8.4 ± 0.4 °C for the 12pin configuration, 7.9 ± 0.4 °C for the 16pin configuration, 8.0 ± 0.4 °C for the 8prism configuration, and 5.7 ± 0.4 °C for the 8pin-NS configuration.

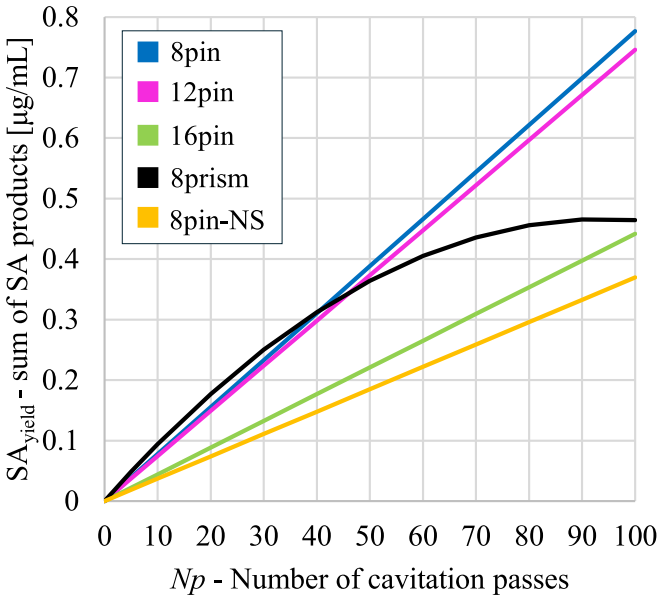

Fig. 3. The sums of concentrations of three major SA products (2,3-DHBA, 2,5-DHBA and 1,2-DHB) with respect to number of passes in the PD-RGHC for the investigated rotor-stator geometries.

The chemical analysis (Table 2) reveals a slight reduction in pH across all configurations, indicative of the release of acidic intracellular components following HC-induced cell lysis. EC increases were also observed, i.e., 14.7 %, 13.7 %, 11.4 %, 9.3 %, and 6.8 % for the 8pin, 12pin, 16pin, 8prism, and 8pin-NS configurations, respectively. This increase may be attributed to improved particle–particle contact, as the overall surface area increased due to particle fragmentation (with smaller particles resulting in higher conductivity and vice versa). The ORP increased in all our cases, indicating that HC-treated sludge became more readily reducible, however, its increase was below the threshold to improve the dewaterability of wastewater sludge as reported before [38].

It is well-established that cavitation of sludge increases its soluble components, commonly evidenced by an increase in sCOD post-treatment [6,7,17,39–41] as intracellular substances are released into the bulk liquid due to HC-induced damage. This trend is observed in the present study as well (Table 2). Furthermore, comparing the 8pin and 8pin-NS configurations reveals that the presence of a stator disc does not enhance sCOD release performance for the 8pin rotor.

Regarding sNH_4, increases of 1.0, 8.5, 2.9, 2.1 and 1.1 mg/l were measured for the 8pin, 12pin, 16pin, 8prism and 8pin-NS configuration, respectively. A similar trend to that of sCOD was noted, again indicating that 8pin and 8pin-NS configurations performed the poorest. The sTP decreased in all cases, suggesting that the soluble fraction was utilized for bonding with other non-soluble components, resulting in an increase of phosphorus in the form of orthophosphate.

The Kruskal–Wallis test was performed to evaluate statistically significant differences among the configurations, revealing statistically significant differences for all the parameters ($p < 0.05$) (details in Suppl. Material 1, Section 1, Table 1.1S). Additionally, to assess the differences on a pairwise level, Dunn's post hoc test was performed (the results of the test are available in Suppl. Material 1, Section 1, Table 1.2S). The analysis identified configurations that were statistically different from the raw sludge for the specific parameters as follows: pH and ORP: 8pin, 12pin, 16pin; EC and PO_4-P: 8pin, 12pin, 16pin; sCOD and sNH_4-N: 12pin, 16pin, 8prism; and sTP: 8pin-NS. For a detailed overview of the statistical differences among all the configurations, please refer to the supplementary material (Suppl. Material 1, Section 1, Table 1.2S).

The One-way PERMANOVA test (Suppl. Material 1, Section 1, Table 1.3S), revealed statistically significant differences among the

Table 2
Change in chemical parameters: pH, EC, ORP, sCOD, sNH_4-N, sTP, PO_4-P. Measurements were performed in triplicate and are presented as mean ± standard deviation. Detailed statistical analyses, including the Kruskal–Wallis test (Table 1.1S), Dunn's post hoc test (Table 1.2S), one-way PERMANOVA (Table 1.3S), and nmMDS analysis (Fig. 1.1S), are provided in Suppl. Material 1, Section 1.

	raw sludge	8pin	12pin	16pin	8prism	8pin-NS
pH (−)	6.97 ± 0.02	6.84 ± 0.02	6.86 ± 0.02	6.87 ± 0.02	6.85 ± 0.02	6.89 ± 0.02
EC (µS/cm)	577 ± 3	661 ± 3	656 ± 3	643 ± 3	631 ± 3	616 ± 3
ORP (mV)	38.5 ± 0.1	46.1 ± 0.1	45.1 ± 0.1	44.1 ± 0.1	45.3 ± 0.1	43.3 ± 0.1
sCOD (mg/l)	90 ± 1	176 ± 2	392 ± 4	410 ± 4	387 ± 8	177 ± 16
sNH_4-N (mg/l)	4.6 ± 0.4	5.6 ± 0.2	13 ± 0.3	7.5 ± 0.9	6.7 ± 0.9	5.7 ± 0.3
sTP (mg/l)	185.4 ± 1.4	157.1 ± 6.9	168.7 ± 1.6	157.5 ± 2.1	158.5 ± 8.0	148.5 ± 14.0
PO_4-P (mg/l)	42.7 ± 1.4	63.8 ± 1.4	65.8 ± 1.7	68.5 ± 3.8	53.6 ± 2.2	58.2 ± 1.4

groups ($p < 0.05$), indicating strong evidence that the overall multivariate dataset differs significantly when all configurations are considered together. However, pairwise comparisons did not detect significant differences between individual pairs of groups. To further explore these findings, a nmMDS analysis was conducted to visualize group clustering, which revealed clear separations among the configurations (Suppl. Material 1, Section 1, Fig. 1.1S).

Disintegration degree (DD) is a key metric for assessing WAS treatment efficiency, reflecting the release of intracellular and extracellular organic matter into the liquid phase. It was calculated using the following formula:

$$DD[\%] = \frac{sCOD_f - sCOD_0}{sCOD_{max} - sCOD_0} \times 100 \quad (1)$$

where $sCOD_f$ is sCOD of treated WAS, $sCOD_0$ is the soluble COD of untreated WAS and $sCOD_{max}$ is the maximum soluble COD determined through the alkaline hydrolysis method [42]. For this, 1 M NaOH (Sigma-Aldrich, Germany) was added to the initial WAS sample in a 1:2 ratio and heated for 10 min at 90 °C. The $sCOD_{max}$ measured was 1803 mg/l.

The alkaline hydrolysis method for measuring $sCOD_{max}$ is widely used [43–47]. However, in some studies on WAS treatment using RGHC, DD is often determined by using TCOD for $sCOD_{max}$. To align our data with these studies [7,9,40], we also applied this method. Additionally, Petkovšek et al. [6] determined $SCOD_{max}$ using chemical treatment using H_2SO_4. To distinguish between these three methods, the following abbreviations will be used: DD_{TCOD}, DD_{H2SO4} and DD_{NaOH}.

Given the relatively short treatment time of approximately 4 min and the lower organic matter content, the calculated DD (Fig. 4) was not as substantial as those reported in other studies. For instance, Petkovšek et al. [6], reported a DD_{H2SO4} of 40.8 % and 57.2 % after 20 passes, while treating 196 L of WAS. Similarly, high values were observed in ultrasonication treatments. Erden and Filibeli [47] reported a maximum DD_{NaOH} of 57.9 % at a specific energy of 9690 kJ/kg TS and a reaction time of 40 min. Interestingly, at higher energy inputs, DD_{NaOH} decreased, likely due to strong radical-induced oxidation resulting in mineralization of soluble organics. Zawieja et al. [44] reported a DD_{NaOH} of 35 % for ultrasonic treatment and 63 % when combined with Fenton's reagent.

Kim et al. [40], with their Advanced RGHC (ARGHC), reported DD_{TCOD} of 42.3 % after 20 passes. However, their method of calculating DD needs to be amended, as it involved normalization of the measured sCOD to compensate for oxidation to allow for comparison with their ultrasonication test. Without the normalization step, their DD values would be much lower, at 7.0 %, 10.1 %, 11.9 % and 13.5 % for 5, 10, 15 and 20 passes, respectively. Further, in a laboratory-scale experiment (40 L) conducted without cooling, Vilarroig et al. [7] achieved a DD_{TCOD} of 26 % with their cavitation generator in a treatment time of 30 min and 22.5 passes, during which the sample reached a temperature of 70 °C. However, when cooling was employed (temperature below 35 °C), which better aligns with our study conditions, DD_{TCOD} was only 2.2 %, 2.8 % and 4.9 % after 37.5, 75 and 112.5 passes, respectively. Additionally, they emphasized that DD values were highly dependent on the quality of the substrate or co-substrate used which supports the lower values reported in the literature. For example, in a pilot scale PD-RGHC study, for the two investigated scenarios, DD_{NaOH} values of 7.7 % and 6.0 % after 30 passes (20 and 18.4 min, respectively) and DD_{TCOD} of 2.0 % and 1.5 % were reported [17]. In a laboratory-scale PD-RGHC study [8] DD_{NaOH} and DD_{TCOD} values of 22.3 % and 5.2 %, were achieved, respectively. Similarly, DD_{NaOH} values of 12.2 % and 11.7 % were reported when treating two different sludge samples in a hydrodynamic disintegrator at 3000 rpm (210 kJ/L) [43]. Low DD_{NaOH} values of 6.4 % were also observed for ultrasonication treatment at a specific energy input of 200 kJ/kg TS [45].

In our preliminary study utilizing WAS with a TS content of 3.7 %, the selection of rotor–stator configurations did not lead to significant differences in solubilization performance [24], which involved WAS. However, our current study revealed that the choice of rotor–stator configuration significantly affects solubilization efficiency for samples with lower TS content, as suggested before [8].

3.3. Changes in UV–Vis spectra and characteristic indices

The analysis of UV–Vis spectra provides critical insights into the structural and compositional changes of CDOM in WAS following HC treatment. By examining spectral trends, characteristic indices, and their ratios based on the work of Helms et al. [33], the extent of organic matter fragmentation, oxidation, and humification processes can be evaluated. These indicators also demonstrate how HC mimics microbial degradation mechanisms, breaking down larger, recalcitrant compounds into smaller, more reactive fragments.

UV spectra, presented in Fig. 5, showed the highest absorbance in the UVC (200–280 nm) and UVB (280–315 nm) ranges. Absorbance decreased monotonically across all samples, stabilizing at 0.2 in the visible range, with minimal sample differences. These results align with previous research [17] and suggest increased dissolved organic carbon (DOC) concentration post-HC treatment [48]. The observed changes in UV–Vis spectra can be primarily attributed to shear and pressure forces generated by the HC treatment, which affect the CDOM and its optical properties. The entire spectra from 200 to 900 nm are provided in Suppl. Material 1, Section 5, Fig. 5.1S, while the baseline-corrected spectra are available in Suppl. Material 1, Section 5, Fig. 5.2S.

The one-way PERMANOVA on the UV spectra (200–400 nm) revealed statistically significant differences among the samples ($p < 0.0005$). Non-metric multidimensional scaling (nmMDS) analysis clearly distinguished between configurations and showed similarities between 8pin and 16pin configurations, as illustrated in Suppl. Material 5, Fig. 5.2S.

In Table 3, E2:E3 and E4:E6, SumA250-450 and the slope ratio (SR) of regions 275–295 nm and 350–400 nm are presented. An increase in the E2:E3 ratio post-HC treatment indicates the fragmentation of larger DOM molecules into smaller fragments [33], a trend observed across all five treatment cases, confirmed by particle size distribution analysis in Section 3.5. The E4:E6 ratio, a marker of humification [33], suggests increased decomposition and transformation of organic matter. This suggests that the effects of HC mimic microbial processes, but within a significantly shorter time frame, leading to the formation of more

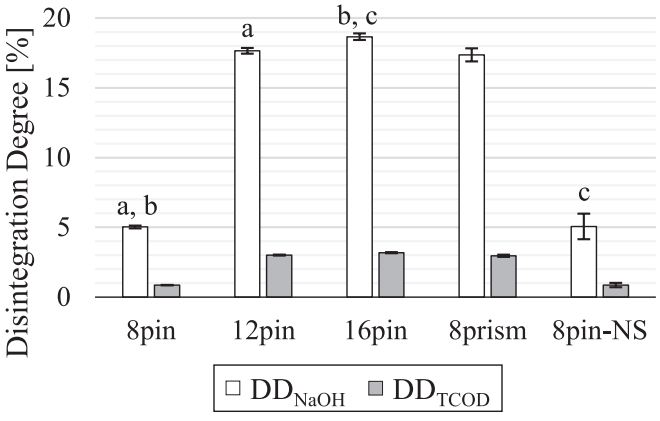

Fig. 4. Comparison of Disintegration Degree (DD) obtained either by chemical disintegration with NaOH (DDNaOH) method or TCOD (DDTCOD) method. Error bars represent one standard deviation. Same letters (a, b, c) designate statistically significant differences between columns within DDNaOH or DDTCOD results based on Dunn's post hoc test ($p < 0.05$), available in Suppl. Material 1, Section 1, Table 1.4S. Columns sharing the same letter differ significantly.

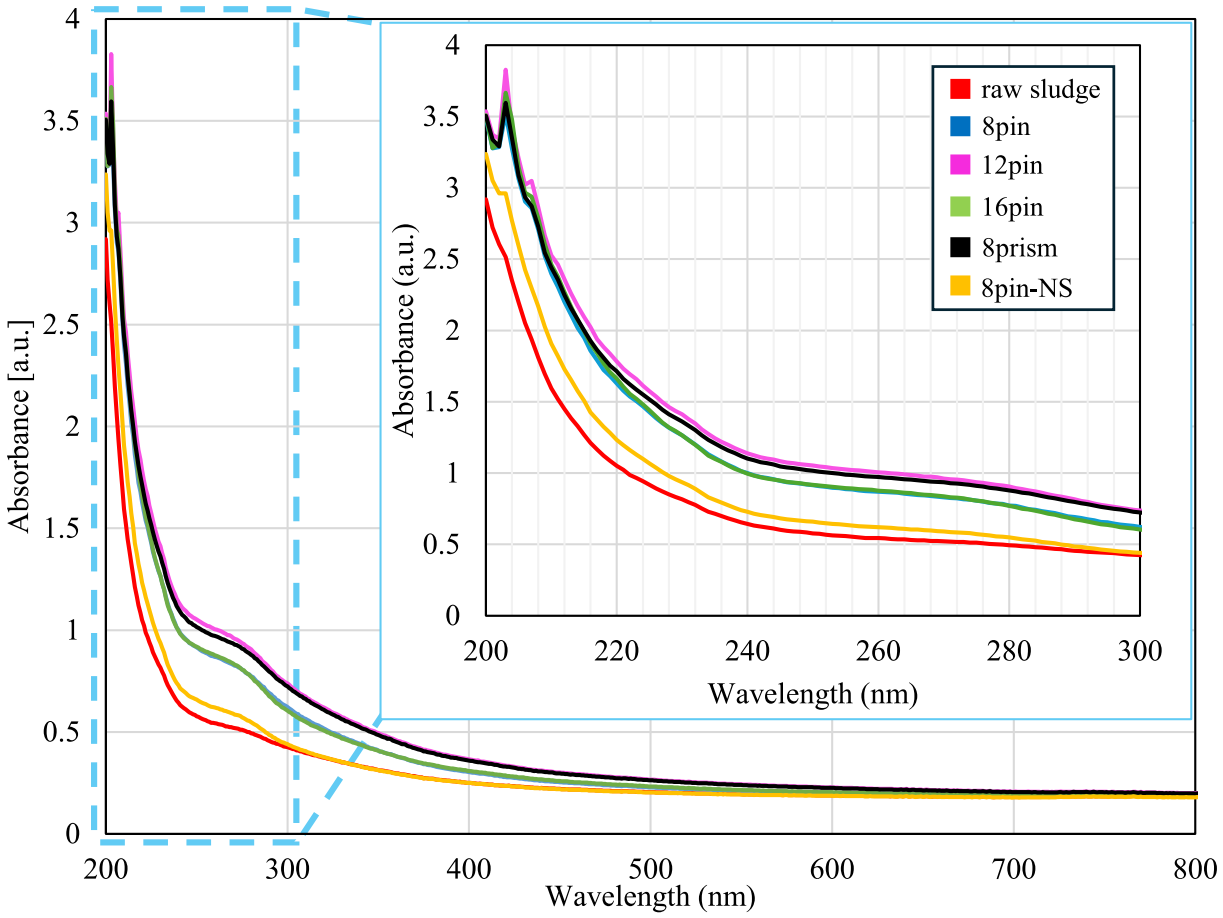

Fig. 5. Absorbance spectra of supernatant in UV–Vis spectra from 200 to 800 nm. The spectra for 8pin and 16pin samples overlap. Baseline-corrected spectra are available in Suppl. Material 1, Section 5, Fig. 5.2S.

Table 3
Characteristic UV–Vis indices. E2:E3: relative size of DOM molecules; E4:E6: humification and aromaticity; SumA250-450: CDOM concentration; S275-295, S350-400 and SR: molecular weight and CDOM degradation. Indices were obtained from triplicate spectra and are reported as mean ± standard deviation. Detailed statistical analyses, including Kruskal–Wallis test (Table 5.1S), Dunn's post hoc test (Table 5.2S), one-way PERMANOVA (Table 5.5S) and nmMDS analysis (Fig. 5.15S), are available in Suppl. Material 1, Section 5.

Config. id.	E2:E3	E4:E6	SumA250-450	S275-295	S350-400	SR
raw sludge	1.89 ± 0.02	1.18 ± 0.06	24232 ± 485	−0.00367 ± 0.0001	−0.00127 ± 0.00005	2.9 ± 0.1
8pin	2.34 ± 0.05	1.30 ± 0.08	33589 ± 1505	−0.0079 ± 0.0004	−0.00210 ± 0.00010	3.7 ± 0.3
12pin	2.22 ± 0.02	1.37 ± 0.06	39843 ± 635	−0.0086 ± 0.0002	−0.00257 ± 0.00004	3.3 ± 0.1
16pin	2.34 ± 0.03	1.31 ± 0.08	33558 ± 806	−0.00891 ± 0.00004	−0.00197 ± 0.00006	4.5 ± 0.1
8prism	2.17 ± 0.18	1.36 ± 0.13	38972 ± 5337	−0.0079 ± 0.0007	−0.00250 ± 0.00050	3.1 ± 0.7
8pin-NS	2.17 ± 0.02	1.19 ± 0.07	25226 ± 420	−0.0058 ± 0.0001	−0.00125 ± 0.00007	4.7 ± 0.3

oxidized and recalcitrant compounds. However, E4:E3 did not increase in the 8pin-NS configuration, indicating inadequate treatment effects to promote the rate of these processes. Furthermore, elevated E4:E6 ratios may also indicate changes in CDOM's aromaticity and molecular size, O:C ratio, C:N ratio and carboxyl content [33,49].

Further, the S350-400 index which is correlated with DOM humification degree [50], indicates alterations in all samples except for the 8pin-NS configuration, consistent with the E4:E6 findings. In contrast, the S275-295 index which is associated with DOM composition and molecular weight [33], revealed changes in all five configurations. The slope ratio (SR), which inversely relates to MW and is unrelated to DOM concentration [51], showed no clear trend, however, did exhibit an increase in post-treatment.

Additionally, nucleic acid characterization indices, A230 (carbohydrates and aromaticity), A260 (DNA and RNA), A280 (proteins) and A320 (colorimetric DOC) were evaluated (Table 4). An increase in A230 after HC treatment suggests elevated levels of non-DNA compounds, while an increased absorbance at A260 indicates higher concentrations of organic compounds such as DNA and RNA as well. A rise in A320 indicated elevated colorimetric DOC levels, and an increase in A280 reflected a higher concentration of proteins and aromatic amino acids in the sample [8,17,52]. The simultaneous increase in the E4:E6 and A280 suggests a shift in the composition of the organic matter. While the overall complexity and aromaticity of the CDOM have decreased, as indicated by the E4:E6, there has been a specific increase in protein content, particularly those containing aromatic amino acids. This rise in protein content could result from several factors, most prominently the decomposition of organic matter, which released more proteins and peptides. Comparison with previous research [17] revealed a similar fold increase for the A230, A260, A280 and A320, with the 12pin and 8prism configurations showing slightly higher values.

For the DNA purity indices (Table 5), DNA1 (A260/A230) and DNA2

Table 4
Characterization of nucleic acid via characteristic wavelength indices and their fold increase and comparison with pilot scale study. A230: carbohydrates and aromaticity; A260: DNA and RNA; A280: proteins; A320: colorimetric DOC. Indices were obtained from triplicate spectra and are reported as mean ± standard deviation. Detailed statistical analyses, including Kruskal–Wallis test (Table 5.1S), Dunn's post hoc test (Table 5.3S), one-way PERMANOVA (Table 5.5S) and nmMDS analysis (Fig. 5.15S), are available in Suppl. Material 1, Section 5.

	Mean – water background				Fold increase			
Config. id.	A230	A260	A280	A320	A230	A260	A280	A320
raw sludge	0.40 ± 0.03	0.30 ± 0.02	0.28 ± 0.02	0.20 ± 0.01	1	1	1	1
8pin	0.85 ± 0.07	0.63 ± 0.05	0.56 ± 0.05	0.35 ± 0.03	2.12	2.07	2.01	1.71
12pin	1.00 ± 0.03	0.77 ± 0.03	0.69 ± 0.02	0.45 ± 0.01	2.49	2.51	2.48	2.21
16pin	0.85 ± 0.04	0.64 ± 0.03	0.55 ± 0.02	0.34 ± 0.02	2.12	2.09	1.99	1.66
8prism	0.95 ± 0.2	0.73 ± 0.16	0.66 ± 0.15	0.44 ± 0.11	2.36	2.41	2.39	2.16
8pin-NS	0.52 ± 0.03	0.38 ± 0.02	0.33 ± 0.02	0.21 ± 0.01	1.30	1.25	1.20	1.02
A2*	0.450	0.268	0.228	0.124	1.44	1.27	1.28	1.23
B2*	0.705	0.451	0.387	0.229	2.26	2.13	2.17	2.28

* Results from Kolbl-Repinc et al. [17] for configuration A2 and B2 (after 30 passes).

Table 5
DNA purity indices. DNA1 (A260/230): DNA/carbohydrates; DNA2 (A260/280): DNA/proteins; DNA3 (A260/A320): DNA/colored DOC (primarily humic substances). Indices were obtained from triplicate spectra and are reported as mean ± standard deviation. Detailed statistical analyses, including Kruskal–Wallis test (Table 5.1S), Dunn's post hoc test (Table 5.4S), one-way PERMANOVA (Table 5.5S) and nmMDS analysis (Fig. 5.15S), are available in Suppl. Material 1, Section 5.

Config id.	DNA1	DNA2	DNA3
raw sludge	0.76 ± 0.08	0.76 ± 0.11	1.5 ± 0.14
8pin	0.74 ± 0.08	0.74 ± 0.13	1.82 ± 0.22
12pin	0.77 ± 0.03	0.77 ± 0.05	1.71 ± 0.07
16pin	0.75 ± 0.05	0.75 ± 0.08	1.9 ± 0.13
8prism	0.77 ± 0.03	0.77 ± 0.05	1.72 ± 0.07
8pin-NS	0.73 ± 0.06	0.73 ± 0.1	1.85 ± 0.16
A2*	0.596	1.175	2.161
B2*	0.640	1.165	1.969

* Results from Kolbl-Repinc et al. [17] for configuration A2 and B2 (after 30 passes).

(A260/A280), no statistically significant differences were detected among the samples. These indices, however, indicate that high levels of non-DNA compounds were present in all samples (DNA1 and DNA2 < 0.9), suggesting the presence of proteins, polysaccharides, or other organic materials. Conversely, changes in DNA3 (A260/A320) were observed post-treatment, indicating a significant increase in nucleic acids predominance, i.e. hence purity, across most samples. This suggests that HC contributed to enhanced elution of nucleic acids into solution (intracellular and extracellular from EPS) and the concomitant reduction of colorimetric DOC, including humic substances or other contaminants that absorb at 320 nm, hence supporting the two-way action of cavitation on organic matter.

The Kruskal–Wallis test revealed statistically significant differences across all indices (E2:E3, E4:E6, SumA250-A450, S275-295, S350-400, SR, A230, A260, A280, A320, DNA1, DNA2 and DNA3). The results of the analysis are provided in Suppl. Material 1, Section 5, Table 5.1S. Additionally, Dunn's post hoc test results for pairwise comparisons between groups can be found in Suppl. Material 1, Section 5, Table 5.2S, Table 5.3S and Table 5.4S. Furthermore, the one-way PERMANOVA test (Suppl. Material 1, Section 5, Table 5.5S) revealed statistically significant differences among the groups ($p < 0.05$). Pairwise comparisons did not identify significant differences between individual pairs. To address this, nmMDS analysis was conducted to visualize group clustering, revealing clear separations among the configurations investigated (Suppl. Material 1, Section 5, Fig. 1.14S).

3.4. Changes in FTIR spectra and characteristic wavelengths

FTIR spectroscopy was used to analyze structural and compositional changes in WAS after HC treatment. By examining characteristic peaks, we offer insights into biochemical transformations, changes to microbial cell structures and the release of organic matter. This helps evaluate HC effects and interactions between hydrodynamic forces and biochemical components. The FTIR spectra of raw and HC-treated samples (Fig. 6) shows similar changes to those reported in our previous work [24], irrespective of different sludge batches. In our case, all FTIR spectra have similar peak positions, but slightly different peak intensities. Specifically, an increase in the peaks at 1648 cm^{-1} (C=O and C–N stretching vibrations of proteins, Amide I) and 1537 cm^{-1} (N–H and C–N stretching in –CO–NH–, Amide II) was associated with amino acids in microbial cell walls [53]. Furthermore, some distinctions were observed in the band characteristic of bacterial cell walls for both Gram-positive and Gram-negative bacteria with its peak at 1234 cm^{-1} [54]. The increased intensities of the bands at 3280 cm^{-1}, corresponding to the O–H stretching vibrations of hydroxyl groups (–OH), suggest a higher presence of carboxylic acids or alcohols [55]. The apparent peaks from 2926 to 2853 cm^{-1}, related to the C–H stretching in CH, CH_2, and CH_3 groups [55], indicate the presence of long-chain hydrocarbons and aliphatic organic compounds. These peaks were evident in all HC-treated samples. In contrast, the raw sludge exhibited similar peaks, but they were shifted to higher wave numbers. This shift was more noticeable in the raw FTIR spectra, as detailed in Suppl. Material 1, Section 6, Fig. 6.1S. Additionally, the intensity of the band due to C–O stretching vibrations at 1050 cm^{-1} increased as well, suggesting the increase of fats and fatty acids in the soluble sample [54]. This improved the availability of the same compounds for recovery through microbial lipid conversion, while also enhancing overall sludge reduction [56]. An increase was also observed in the intensity of the band with its peak at 1408 cm^{-1}, characteristic of C=O symmetric stretching in the protonated carboxyl group [55]. Different HC treatments caused differences in concentrations of functional groups, similar to the study of Yang et al. [57].

The intensity of the bands associated with microbial and bacterial cell walls (1648 and 1537 cm^{-1}) was highest for the 8prism configuration, which also exhibited the greatest pressure fluctuations and cavitation cloud coverage [24,27]. SA dosimetry showed that 8prism, 8pin and 12pin configurations generated similar concentrations of $^{\bullet}OH$ (Fig. 3). However, the 8pin and 12 pin were operated at lower pressures, suggesting that hydrodynamic conditions were the primary factor influencing cell wall damage. In contrast, the 16pin configuration had lower effective pressure, due to diminished cavitation cloud development, while the 8pin-NS configuration, lacking a stator, failed to generate the necessary pressure fluctuations for aggressive cavitating conditions.

3.5. Analysis of particle size distribution, interfacial tension and capillary suction time

Particle size is a critical parameter for assessing the efficiency of

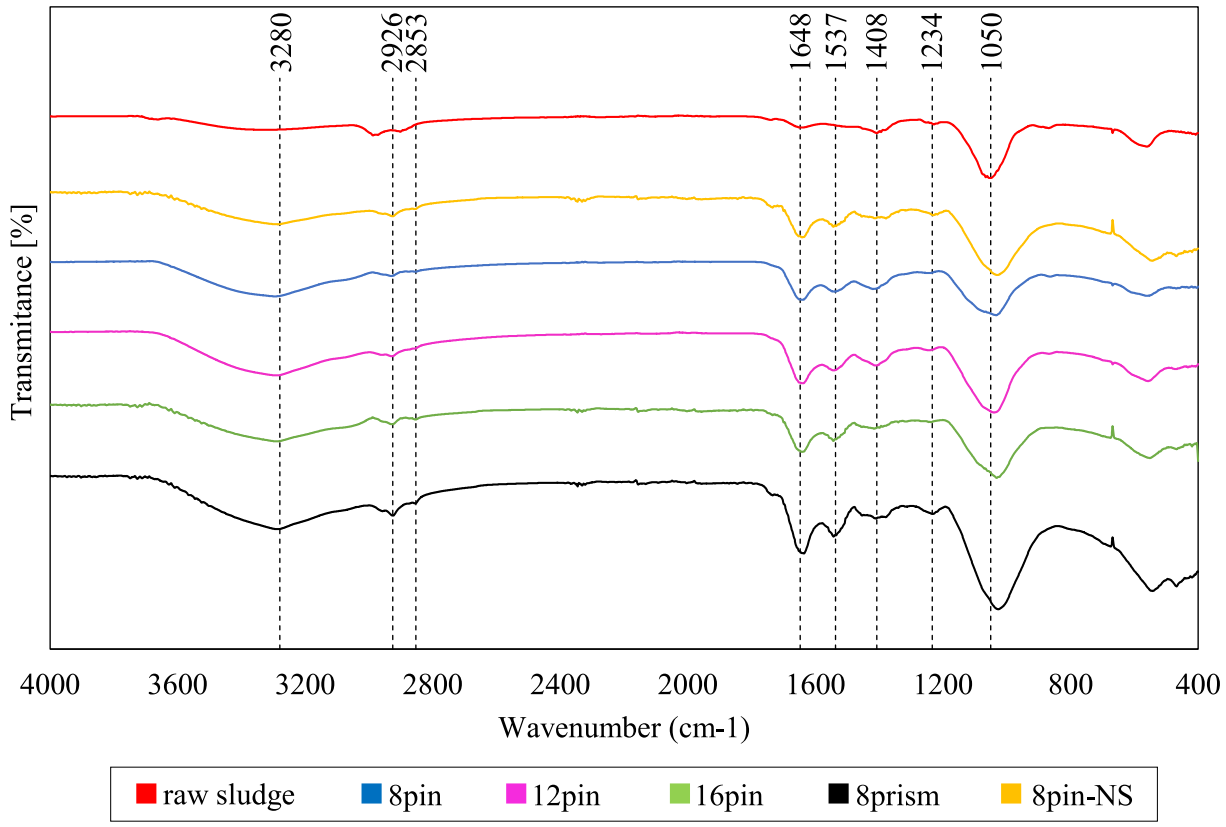

Fig. 6. FTIR spectra characteristic wavenumbers. 1050 cm^{-1}: Fatty acids; 1234 cm^{-1}: Bacterial cell walls of Gram-positive and Gram-negative bacteria;1408 cm^{-1}: Humification and organic matter decomposition; 1648 cm^{-1} and 1537 cm^{-1}: Amino acids in microbial cell walls; 2853 cm^{-1}: Aliphatic organic compounds; 2926 cm^{-1}: Long-chain hydrocarbons; 3280 cm^{-1}: Carboxylic acids or alcohols.

sludge treatment. Smaller particle sizes can enhance biodegradability and facilitate downstream processes. The comparison of particle size distribution, interfacial tension and capillary suction time helps identify the degree of sludge disintegration and its impact on dewaterability. Particle size distribution curves $Q_3(x)$ and $dQ_3(x)$ (Fig. 7) reveal effective particle fragmentation across all five configurations, with reductions in d_{10}, d_{50} and d_{90} values detailed in Table 6. All configurations exhibit similar reduction efficiency. However, consistent with Blagojević et al. [24], the 8pin-NS setup showed less consistency, evidenced by an additional peak at 1000 μm in the $dQ_3(x)$ curve. A similar pattern was observed for the 8pin regime. This multimodal distribution indicates that while larger particles contribute to the overall volume, smaller particles dominate the 90 % mark.

For the 8pin, 12pin, 16pin, and 8prism configurations, D(4,3) was

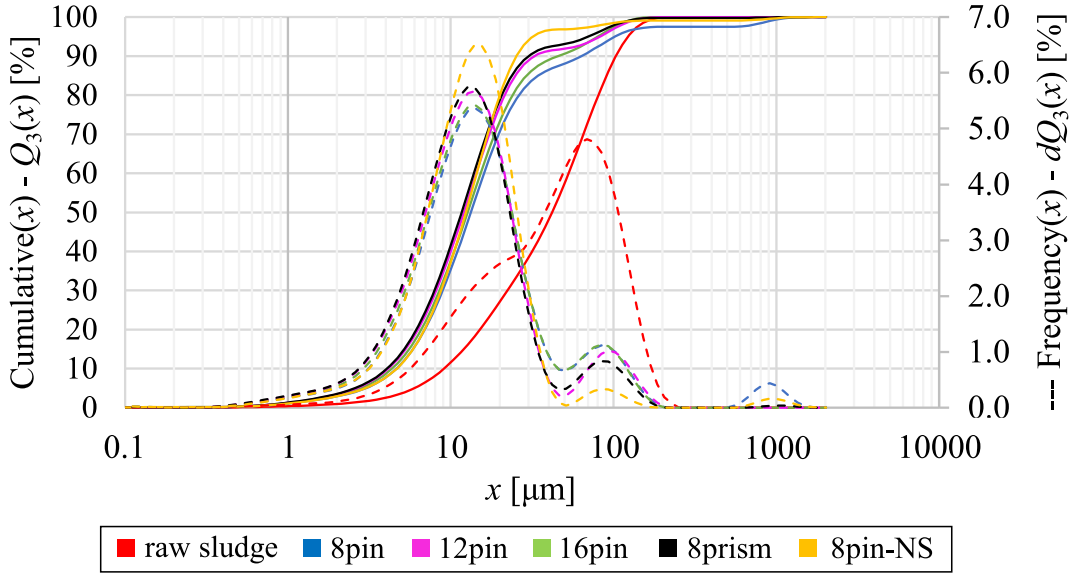

Fig. 7. Particle size distribution curves. Solid lines represent cumulative particle size distribution, Q3(x), while dashed lines represent differential particle size distribution, dQ3(x).

Table 6
Particle size distribution parameters (d_{10}, d_{50}, d_{90}, D(4,3), Mode, Median, Span and Spec. Surface Area), IFT and CST. The values are reported as mean ± standard deviation. Detailed statistical analyses, including the Kruskal–Wallis test (Table 1.5S) and Dunn's post hoc test (Table 1.6S), along with a discussion of the results, are provided in Suppl. Material 1, Section 1.

parameter	unit	raw sludge	8pin	12pin	16pin	8prism	8pin-NS
d_{10}	µm	9.3 ± 1.1	4.6 ± 0.4	4.4 ± 0.2	4.2 ± 0.3	4.1 ± 0.2	4.7 ± 0.1
d_{50}	µm	42.1 ± 6.1	13.3 ± 1.4	12.8 ± 1.1	12.1 ± 1.1	11.8 ± 0.9	12.4 ± 0.5
d_{90}	µm	103 ± 11.7	53 ± 25.7	47.9 ± 19.4	43.2 ± 25.1	38.6 ± 20	25.8 ± 2.4
$D(4,3)$	µm	49.9 ± 6.1	21.6 ± 6.3	20.4 ± 4.2	19.3 ± 5.5	19.5 ± 7.1	23.3 ± 17.4
Mode	µm	66.8 ± 6.5	13.3 ± 0.6	13.1 ± 0.5	13.1 ± 0.5	12.7 ± 0.4	13.9 ± 0.5
Median	µm	42.1 ± 6.1	13.3 ± 1.4	12.1 ± 1.1	12.1 ± 1.1	11.8 ± 0.9	12.4 ± 0.5
Span	–	2.2 ± 0.2	3.5 ± 1.6	3.1 ± 1.7	3.1 ± 1.7	2.8 ± 1.5	1.7 ± 0.1
Spec. Surface Area	cm^2/cm^3	3373 ± 349	7737 ± 608	8310 ± 594	8310 ± 594	8530 ± 539	8256 ± 499
IFT	mN/m	46 ± 0.1	51.1 ± 0.1	51.3 ± 0.1	52.9 ± 0.1	54.6 ± 0.1	53.8 ± 0.1
CST	s	24 ± 1	455 ± 13	627 ± 58	554 ± 37	450 ± 12	345 ± 35

reduced by factors of 2.3, 2.4, 2.6, and 2.6, respectively, while the 8pin-NS configuration achieved a reduction factor of 2.1. The D(4,3) measurement for the 8pin-NS indicated that a significant portion of particles remain relatively large, which may impact the consistency and uniformity of the WAS treated. This could influence performance in applications such as filtration or sedimentation processes.

Comparing particle sizes with sCOD values reveals that the configurations with the least consistency, 8pin and 8pin-NS exhibited the lowest sCOD release. This raises concerns about the effectiveness of the 8pin rotor in enhancing sludge solubilization.

An increase in IFT was accompanied by an increase in CST, suggesting enhanced release of EPS during cavitation, Table 6. The raw sludge had a surface tension of 46 mN/m, which increased to over 50 mN/m post-HC treatment across all configurations. This increase in IFT is attributed to changes in particle size distribution: the reduction of larger particles and the increase of smaller ones reduces voids between particles, thereby enhancing contact area and strengthening intermolecular bonds, adhesion, and cohesion forces within the sludge flocs [58,59].

The CST parameter (Table 6) is a crucial indicator for understanding the impact of HC on WAS filterability. The measured CST values reveal a significant deterioration in filterability after treatment, with post-cavitation values exceeding the typical drying bed threshold of 300 s [60]. The 12pin configuration exhibited the highest CST increase, with a factor of 26.3. The 16pin configuration followed with a factor of 23.2, while the 8pin and 8prism cases increased by factors of 19.1 and 18.9, respectively. The smallest increase, a factor of 14.4, was observed for the 8pin-NS case, reflecting its lower cavitation extent and consequently smaller cell secretions compared to other configurations.

These results raise concerns about installing RGHCs before the dewatering process. However, it is important to consider that CST measurements may not reliably indicate sludge dewaterability in systems using centrifugation, as fine particles infiltrating filter media can cause clogging and increase CST values. Ruiz Hernando et al. [21] found that despite increased CST values following ultrasound treatment, sludge dewatering efficiency via centrifugation was notably improved. Additionally, improved dewaterability due to the release of intracellular water and EPS-bound water, which can be altered with HC was reported before [61].

It is also important to consider the effect of partial oxidation on CST values. Oxidizing certain compounds can increase their hydrophobicity, potentially worsening CST values. However, if these compounds are fully oxidized to CO_2, CST might improve. This hypothesis is supported by studies where external oxidants such as O_3 and H_2O_2 were used, which suggested potential improvements in CST [62,63]. Achieving optimal performance requires careful control of power density and treatment time. A treatment that is too short may only affect less cohesive flocs, leaving stable cellular structures intact. Conversely, an overly long treatment can excessively disrupt sludge cells, releasing substantial amounts of proteins and polysaccharides that could negatively impact dewatering performance [64]. This warrants further investigation, particularly attributed to the release of interstitial and vicinal water.

3.6. Rheological analysis: Changes in flow curves and linear viscoelastic behavior

Understanding how WAS responds to external forces is crucial for its handling, transport, pumping, and dewatering. Knowledge of its rheological properties can inform the design and optimization of treatment processes, while changes in its viscoelastic properties after treatment can reveal improvements or deterioration in its structure and behavior. Overall, the rheological properties of WAS are well known. It is a non-Newtonian multiphase fluid that consists of colloidal matter, EPS and 4 types of water: free water, interstitial water, surface or vicinal water and internal water [65]. WAS is characterized by shear-thinning and thixotropic behavior, polymer-like behavior at low shear rates and thixotropic colloidal suspension-like behavior at high shear rates [29]. Additionally, at TS concentrations below 10 %, some WAS samples may show flow curves indicative of both pseudoplastic and dilatant behavior [66]. Its rheological properties are strongly linked to the amount of Total Suspended Solids (TSS), particle size distribution, surface energy, dewaterability and EPS content [67]. Additionally, the surface charge of WAS significantly affects its stability and rheological properties by influencing the physicochemical interactions between bacteria and inorganic components [68].

The first analysis aimed to evaluate how HC treatment affects the flow behavior of WAS, particularly at different shear stress levels. Fig. 8 demonstrates the apparent viscosity as a function of shear stress for both cavitated and non-cavitated samples, all displaying shear-thinning behavior. HC treatment caused a permanent alteration to the

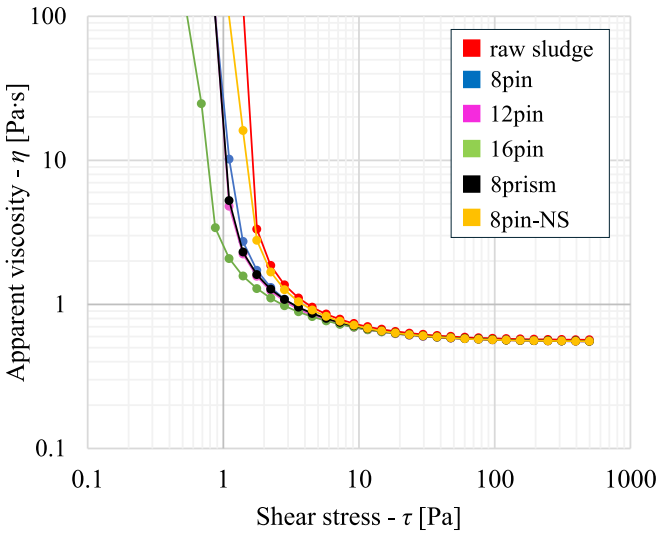

Fig. 8. Apparent viscosity as a function of shear stress.

rheological properties of WAS, with a pronounced reduction in apparent viscosity at low shear stress across all configurations. This reduction is significant as lower apparent viscosity can improve the efficiency of subsequent handling and treatment processes. Furthermore, this observation aligns with findings that apparent viscosity of WAS decreases with the amount of introduced ultrasonication-specific energy [18,20]. The reduction in apparent viscosity is most significant at lower shear rates, while at higher shear rates, where mechanical forces are greater, the effect of sonication is known to be less significant [20]. This reduction in viscosity can be primarily attributed to HC-generated shear and pressure forces, which sever bonds between individual particles, causing permanent structural damage to the sludge matrix and reducing particle size [69]. The temperature effect on WAS [70] further promotes a reduction in viscosity; as the thermal motion of particles becomes more violent at higher temperatures, the network strength between particles weakens more easily. Finer particles then occupy the gaps between larger ones, facilitating effective lubrication and further reducing viscosity. The measured SA_{yield} confirms the presence of $^{\bullet}OH$, indicating that the extreme conditions necessary for their generation were indeed achieved. This suggests that the temperature effect, to some extent, could be responsible for the reduction in viscosity.

The 8pin-NS configuration, characterized by the lowest extent of cavitation, exhibited the smallest reduction in viscosity, consistent with previous findings [24]. This suggests that macro-scale shear alone (as in the 8pin-NS) is less effective than the combination of micro and macro-scale shear in modifying rheological properties. Further evidence is provided by comparing configurations with cylindrical CGUs on the rotor disc; the decrease in apparent viscosity is more significant with an increasing number of rotor pins, indicating more shear zones per rotation. The 8prism configuration's viscosity reduction lies between those of the 8pin and 12pin cases, underscoring the impact of shear zones on viscosity reduction.

Overall, the differences in viscosity are not substantial, suggesting that larger particles likely influence the results at lower shear rates/stresses. The D(4,3) values further support this claim, with the 8pin-NS and raw sludge exhibiting similar values (considering the standard deviation of the 8pin-NS), while the D(4,3) values for other configurations are notably smaller. At higher shear rates/stresses, the aggregates/flocs break apart, resulting in similar viscosity values. Once shear stresses exceed 10 Pa, the floc structures are fully disrupted leading to comparable apparent viscosity values across all samples, approximately 0.57 Pa·s. The infinite viscosity (η_∞), determined at a shear rate of 1000 s^{-1}, where sludge reaches ultimate stabilization after complete disruption, remained consistent across all samples.

The viscoelastic properties of the samples, presented in the form of storage (G') and loss modulus (G'') were measured at shear strains ranging from 1 to 100 % and a constant frequency of 1 Hz, Fig. 9. A greater decrease in G' for the raw sludge sample implies that with HC sludge integrity has been irreversibly altered and that sludge flocs have been damaged. Consequently, less energy can be stored in the sludge matrix when exposed to external forces, meaning smaller elastic recovery. The largest drop in G' was measured for the 8pin-NS configuration, then followed 8pin and 12pin configuration. Regarding the 16pin and 8prism cases, there was an overlap between the untreated samples. From 20 % shear strain onward, the overlap was not present.

As for G'', in the LVE range, all measured values for cavitated samples were lower than raw sludge, indicating impaired energy dissipation capabilities due to irreversible structural damage. G'' for the HC-treated samples was constant until the shear strain exceeded 40 %, beyond this point G'' started to decrease. For the raw sludge sample, G'' began to decrease from its constant value at an earlier point, specifically at 10 % shear strain. In the non-LVE range, the reduction in G' was more pronounced than that of G'', indicating that viscous behavior dominated over elastic behavior. A decrease in G'' post-HC treatment indicates a reduction in the material's ability to store elastic energy, suggesting a decrease in its stiffness or solid-like behavior due to the weakening of intermolecular bonds and disruption of structural integrity.

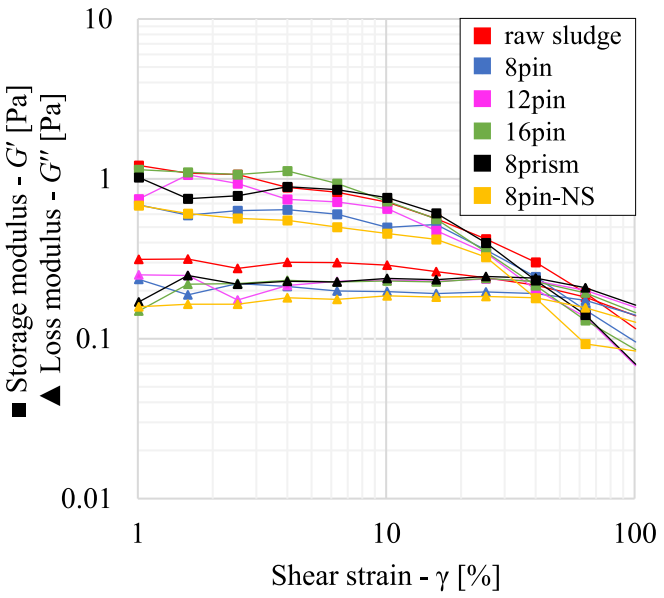

Fig. 9. Amplitude sweep test – Determination of LVE range, storage and loss modulus as a function of shear strain. Performed under destructive conditions like the flow test, but with oscillatory input. Differences in sample consistency, likely due to heterogeneity, are more pronounced at lower loads. At higher deformations, where aggregates/flocs break apart, these differences diminish.

The $G'=G''$ method was used for the determination of yield stress [35]. At the yield stress point, the viscous and elastic contributions are equal. Increasing the stress applied to the sample beyond this point will lead to a state of flow. The presented graph in Fig. 10, displays the yield stress points for the measured samples. It is noteworthy that the intersection point undergoes a leftward shift after the HC treatment, meaning cavitated samples transition from predominantly elastic to predominantly viscous behavior at lower shear stresses. Interestingly, the 16pin, 12pin, and 8prism configurations yielded similar results concerning the alteration of the intersection point. The 8pin and 8pin-NS configurations showed comparable yield stress values, consistent with their d_{10} parameters. In contrast, the raw sludge with the smallest yield stress exhibited the highest d_{10} value.

Suppl. Material 1, Section 7 includes the viscoelastic properties of sludge in the LVE range from a frequency sweep test, revealing stronger elastic behavior ($G' > G''$). The results indicate that HC treatment generally improves elastic behavior and reduces damping, suggesting a more homogeneous and ordered structure, potentially enhancing decomposition efficiency in the AD process.

3.7. Assessing the influence of radicals and correlations among parameters

In the following statistical analysis, measured physicochemical parameters, particle size distribution parameters, UV–Vis characteristic indices, FTIR characteristic peaks, SA_{yield}, absolute pressure and flow rate were used to elaborate on the correlations between these parameters.

To visualize the differences and similarities in the effects of the investigated rotor–stator designs on WAS, these parameters were used in nmMDS analysis (Fig. 11). The 8pin, 16pin, and 8prism configurations cluster closely together, suggesting that their effects on WAS are quite similar. In contrast, the 12pin configuration is more distant, indicating a notable difference in its impact on WAS physicochemical properties compared to the other designs. The 8pin-NS configuration, which is known to produce fewer radicals, appears positioned near the raw sludge, implying that its treatment effect is less significant. A subsequent

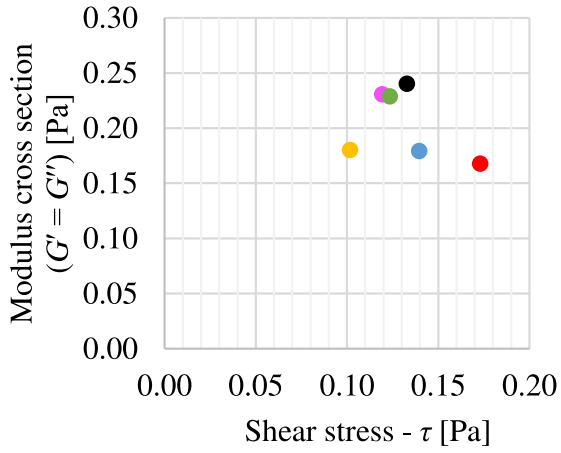

Config. id.	Shear Stress [Pa]	Yield Stress ($G' = G''$) [Pa]
raw sludge	0.1729	0.1678
8pin	0.1395	0.1793
12pin	0.1192	0.2308
16pin	0.1234	0.2289
8prism	0.1328	0.2403
8pin-NS	0.1016	0.1801

Fig. 10. Modulus cross section obtained from the amplitude sweep test results (presented in Fig. 9).

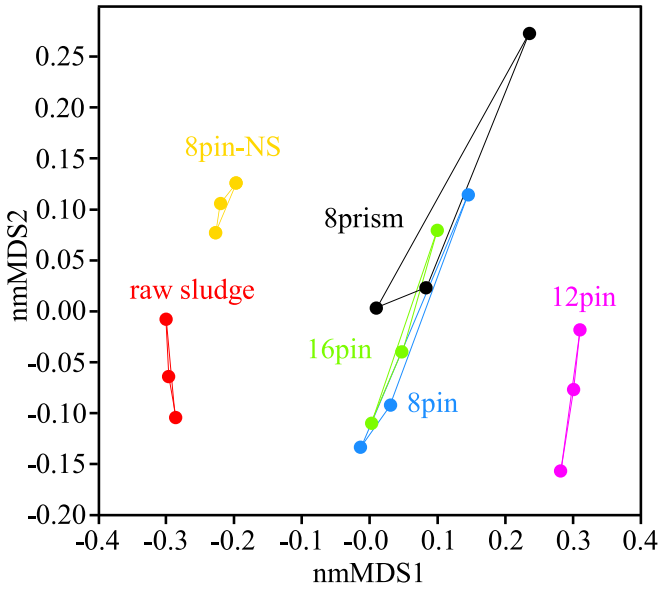

Fig. 11. The nmMDS plot of measured parameters for the investigated rotor–stator designs. The corresponding Shepard plot is available in Supplementary Material 1, Section 7, Fig. 7.1S.

one-way PERMANOVA revealed statistically significant differences between the investigated designs ($p < 0.0001$). For further details, refer to Suppl. Material 1, Section 7.

Additionally, to assess the role of radicals in the treatment process, Pearson's (r) multivariate correlation statistic test was carried out to reveal linear correlations between SA_{yield} (attributed to overall radical production) and other measured parameters in this study. For the graphical representation and calculated values of the correlations between these parameters, refer to Suppl. Material 1, Section 7, Fig. 7.2S. The exact values can be found in the correlation table in Suppl. Material 2 (Excel file). For the SA_{yield}, several statistically significant correlations ($p < 0.05$) were observed, indicating that radicals significantly influence the treatment process. Specifically, strong positive correlations were found with parameters such as PO_4-P ($r = 0.89$), IFT ($r = 0.74$), CST ($r = 0.9$), SSA ($r = 0.85$), and all UV–Vis characteristic wavelengths ($r > 0.86$); and UV–Vis characteristic indices: DNA3, E2:E3 and E4:E6 ($r > 0.82$); DNA1 ($r > 0.74$). On the other hand, DNA2 and SR did not show any statistically significant correlations. Strong negative correlations were noted with particle size parameters, including $D(4,3)$, mode, median, d_{10}, and d_{50} ($r < -0.86$), and spectral slopes S275-295 and S350-400 ($r < -0.85$). Moreover, for parameters like p_{abs} and Q, statistically significant correlations with UV–Vis characteristic indices were limited to DNA3 and E2:E3 ($r > 0.83$). Given that SA_{yield} showed strong correlations with most UV–Vis indices these findings suggest that the observed changes in UV–Vis characteristics are predominantly attributed to the effects of radicals rather than the hydrodynamic flow conditions. The results obtained for the UV–Vis characteristic wavelengths also align with the correlations observed between measured sCOD and UV–Vis absorbance scans at wavelengths of 290, 270, 260, 254, 245, 240, and 220 nm, as reported by Waltham and Örmeci [71]. The present study reveals a strong, statistically significant relationship between sCOD and these UV–Vis characteristic wavelengths ($R^2 > 0.8$). For further details, see Suppl. Material 1, Section 5, Fig. 5.7S–5.14S. Surprisingly, Pearson's (r) correlation test revealed no statistically significant correlation between sCOD and SR. Further examination revealed that most UV–Vis characteristic indices exhibited strong positive correlations with sCOD, DD_{NaOH}, and CST ($r > 0.8$), positive moderate correlations with NH_4-N ($r > 0.75$) and PO_4-P ($r > 0.64$), and negative moderate correlations ($r < -0.6$) with mode, median and d_{50}, all being statistically significant ($p < 0.05$). For the FTIR spectra, statistically significant correlations were observed for the peak at 3280 nm, associated with O–H stretching vibrations of hydrocarbons (Carboxylic acids or alcohols) [55]. This peak showed strong positive ($r > 0.87$) statistically significant correlations with $D(4,3)$, mode, median, d_{10} and d_{50}, and strong negative correlations with IFT ($r < -0.84$), SSA ($r < -0.91$); p_{abs} and Q ($r < -0.88$). The analysis of microbial cell wall changes, indicated by FTIR peaks 1537 cm^{-1} (N–H and C-N stretching in –CO-NH-, Amide II) and 1648 cm^{-1} (C=O stretching in Amide I), revealed strong negative statistically significant correlations ($r < -0.82$) with both p_{abs} and Q. Although SA_{yield} also showed negative correlations ($r = -0.6$) with these peaks, they were not statistically significant ($p = 0.041$ and 0.048, respectively). These findings suggest that hydrodynamic flow conditions within the reactor were the primary factors influencing microbial cell wall changes, with a potential synergistic effect from radicals warranting further investigation.

Spearman's (rs) correlation test (Suppl. Material 2) revealed the following statistically significant correlations: strong positive ($r > 0.76$) correlations between SA_{yield} and the parameters sCOD, NH_4-N, and DD_{NaOH}; a strong negative ($r = -0.94$) correlation between p_{abs} and FTIR 1234 cm^{-1} (associated with bacterial cell walls of Gram-positive and Gram-negative bacteria) (Wiercik et al., 2022a); and strong positive ($r = 0.89$) correlations between flow rate and the parameters sCOD and DD_{NaOH}, suggesting that some correlations might be nonlinear.

Additional analysis, incorporating viscosity curves into the existing Pearson's (r) table (Suppl. Material 2), revealed the following findings. Consistent with our past research [24], statistically significant

correlations were identified between viscosity at low shear stresses and several key parameters: sCOD ($r < -0.83$), CST ($r < -0.92$), and $D(4,3)$ ($r > -0.80$). Contrary to the earlier findings on more concentrated WAS [24], no statistically significant correlations were observed with other particle size distribution parameters, except for d_{10} ($r > 0.81$; across the entire curve), and for d_{50} ($r > 0.75$) and SSA (strong negative; $r < -0.74$) in the higher shear stress regions. At low shear stresses, additional correlations were observed with DD_{NaOH} ($r < -0.75$) and PO_4-P ($r < 0.80$) across the entire measured range. Statistically significant negative correlations ($r < -0.76$) were also noted with most UV–Vis indices (A220, A230, A240, A245, A254, A260, A270, A280, A290, DNA1, E2:E3, E4:E6, SumA250-450), while S275-295 exhibited a strong positive correlation ($r > 0.83$). These findings suggest that changes in rheological properties are closely linked to changes in DOM humification, aromaticity, and molecular size of CDOM, as well as DNA and RNA. This supports the previous statement that cell secretions significantly influence the overall rheological properties [24]. Across the entire flow curve, statistically significant correlations were observed with E2:E3 ($r < -0.89$), PO_4-P ($r < -0.80$; across most of the curve), and d_{10} ($r > 0.81$). In the low shear stress zone, additional correlations were found with S275-295 ($r < -0.81$). At higher shear stresses, statistically significant correlations were found with IFT ($r > 0.82$), mode ($r > 0.83$), median ($r > 0.80$), SSA ($r < -0.82$), d_{50} ($r > 0.80$), DNA3 ($r < -0.82$), SA_{yield} ($r < -0.82$), p_{abs} ($r < -0.84$), Q ($r < -0.82$), and FTIR 3280 cm^{-1} ($r < -0.81$) (indicative of carboxylic acids or alcohols). Further, Spearman's (rs) correlation test (Suppl. Material 2) revealed additional strong negative ($r < -0.89$) statistically significant correlations with sCOD, NH_4-N and DD_{NaOH} suggesting potential nonlinearity. The inclusion of data from amplitude and frequency sweep tests did not reveal any new correlations.

These findings underscore the complex interplay between various physicochemical parameters and radical production in HC treatment. However, in the future, more data is needed to better understand the underlying mechanisms and optimize these processes. Future research should focus on a detailed analysis of the synergistic effects between radicals and hydrodynamic flow conditions, as well as the implications of these findings for large-scale applications.

4. Conclusion

The study evaluated the impact of HC treatment on WAS with 0.7 % TS content using a laboratory-scale PD-RGHC. The findings highlight statistically significant changes in the physicochemical and rheological properties of WAS post-treatment. Chemical analysis confirmed an increase in soluble components and alterations in various physicochemical parameters, with notable effects on sludge filterability and viscosity. Overall, PD-RGHC treatment shows promise in improving the manageability of WAS, with potential benefits for wastewater treatment operations, despite the challenges associated with increased filterability and operational considerations.

The differences in WAS parameters between the individual rotor–-stator configurations in this study (TS 0.7 %) are more pronounced and statistically significant compared to those observed in WAS with a TS content of 3.7 % [24]. This finding suggests that the effectiveness of specific configurations varies more substantially at lower TS content, offering valuable insights for future optimization efforts and providing guidelines to plant operators.

SA dosimetry revealed that radical production performance up to 50 passes was quite similar for the 8pin, 12pin, and 8prism configurations. Beyond 50 passes, the 12pin and 16pin configurations demonstrated superior performance compared to the 8prism. Notably, the radical production with the 16pin and 8pin-NS configurations was approximately 50 % lower, with the 8pin-NS performing the least effectively.

DD increased for all five regimes, with 12pin, 16pin and 8prims configurations showing the most promise (>17 %). These three configurations produced twice the SA_{yield} of the other two (8pin and 8pin-NS) and achieved a DD three times higher (>17 % compared to 5 %). HC treatment resulted in a considerable increase in CST, indicating a deterioration in filterability (increased by a factor of 14.4) possibly due to smaller particles clogging filter pores. Regarding dynamic viscosity, the greatest reduction was observed with the rotor disc featuring the largest number of pins, specifically the 16pin configuration. A similar result was reported in a previous study on WAS with TS content of 3.7 % [24], indicating the superiority of this configuration in reducing apparent viscosity compared to other regimes. Additionally, a reduction in apparent viscosity and modifications G' and G'' were observed, reflecting structural changes in the sludge. These changes, particularly the drop in apparent viscosity, are advantageous for sludge pumping and handling processes.

Statistically significant correlations were reported between radical concentration and UV–Vis characteristic indices (excluding DNA2 and SR), revealing that radicals are responsible for inducing changes to DOM humification, aromaticity and molecular size of CDOM, DNA and RNA. Statistically significant correlations were also reported between radical concentration and the following parameters: PO_4-P, IFT, CST, $D(4,3)$, mode and median. Changes in microbial cell walls were attributed to hydrodynamic conditions in the reactor as revealed by strong negative statistically significant correlations between peaks at 1537 cm^{-1} and 1648 cm^{-1} and p_{abs} and Q. Although radical concentration showed negative correlations with these peaks, the correlations were not statistically significant. This suggests that hydrodynamic forces were the main drivers of cell wall changes, with a possible synergistic effect from radicals.

The measured BMP of WAS were within the limits given in the study by Murovec et al. [72]. In our case, no increase in methane yield was achieved by pre-treatment (Suppl. Material 1, Section 3, Fig. 3.1S and 3.2S) most probably due to the oxidation of labile carbon. Further discussion is given in the Suppl. Material 1, Section 3.

The study underscores the critical role and importance of radicals in the HC treatment process and provides insights for further optimizing the PD-RGHC setup to enhance treatment effectiveness. Future research will focus on investigating the biomethane yield for WAS with similar TS content and evaluating the energy balance. The goal is to further improve the sustainability and efficiency of this device in wastewater treatment processes.

Declaration of generative AI and AI-assisted technologies in the writing process

During the preparation of this work the authors used ChatGPT 4.0 to improve readability and language. After using this tool/service, the authors reviewed and edited the content as needed and take full responsibility for the content of the published article

Funding

The authors acknowledge the financial support from the Slovenian Research Agency ARIS research programs P2-0422 "Functionalized fluids for advanced energy systems", P2-0401 "Energy Engineering", and P2-0180 "Water Science and Technology, and Geotechnical Engineering: Tools and Methods for Process Analyses and Simulations, and Development of Technologies" and grants J2-4480 "Removal of selected antimicrobials by plasma-cavitation technology from water matrices of varying complexity (Causma) and L7-4422 "UPTAKE": Agricultural reuse of wastewater and sewage sludge: uptake and distribution of contaminants of emerging concern in tomato plant as a model; J7-50152 Decontaminated biochar from sewage sludge as an efficient soil fertilizer and conditioner; J2-3056 Development of an optical measuring method for measurement of the turbulent two-phase flow with free surface. The REMEDIES project (HORIZON-MISS-2021-OCEAN-03-01), grant agreement No. 101093964, the CAVIPHY project (ERC -2022-POC1) grant agreement No. 101069228 and CABUM project (ERC-2017-COG) grant agreement No. 771567, the project UPSTREAM (HORIZON-MISS-2022-OCEAN-01-04) grant agreement ID: 101112877.

CRediT authorship contribution statement

Marko Blagojevič: Writing – review & editing, Writing – original draft, Visualization, Validation, Methodology, Investigation, Formal analysis, Conceptualization. **Mojca Zupanc:** Supervision, Project administration, Investigation. **Jurij Gostiša:** Resources. **Blaž Stres:** Writing – original draft, Supervision, Formal analysis. **Alenka Šmid:** Investigation. **Matevž Dular:** Supervision, Formal analysis. **Lidija Slemenik Perše:** Writing – original draft, Resources. **Urška Gradišar Centa:** Writing – original draft, Resources, Formal analysis. **Benjamin Bizjan:** Resources. **Gašper Rak:** Resources, Project administration. **Uroš Novak:** Resources. **Blaž Likozar:** Writing – original draft, Supervision, Formal analysis. **Sabina Kolbl Repinc:** Writing – review & editing, Writing – original draft, Supervision, Project administration, Methodology, Investigation, Formal analysis, Conceptualization.

Declaration of competing interest

The authors declare that they have no known competing financial interests or personal relationships that could have appeared to influence the work reported in this paper.

Acknowledgments

The authors express their gratitude to the Central Wastewater Treatment Plant Ljubljana for providing the necessary samples for our experiments. We also extend our sincere thanks to Matic Šobak from the Faculty of Mechanical Engineering for his help with the rheology measurements and to Renato Babič for his valuable assistance with the measurements of the WAS physicochemical properties. Additionally, we thank Dragana Ribič and Donya Allahbakhshi Hafshejani for their support with the FTIR measurements. The authors acknowledge the support of D13 (Department of Catalysis and Chemical Reaction Engineering), National Institute of Chemistry and its members for support, access to analytical methods and fruitful discussions.

Appendix A. Supplementary data

Supplementary data to this article can be found online at https://doi.org/10.1016/j.ultsonch.2025.107291.

References

[1] J. Lu, Q. Lu, Q. Hu, B. Qiu, Recovery of organic matters by activated sludge from municipal wastewater: Performance and characterization, Environ. Res. 252 (2024) 118829, https://doi.org/10.1016/j.envres.2024.118829.
[2] J. Ke, S. Zhu, W. Chen, Y. Song, Y. Liu, R. Guo, J. Chen, Resource utilization of chemical excess sludge to produce metal–organic framework with outstanding Fenton-like performance for sulfamethoxazole removal, Chem. Eng. J. 496 (2024) 154140, https://doi.org/10.1016/j.cej.2024.154140.
[3] U. Neis, K. Nickel, A. Tiehm, Enhancement of anaerobic sludge digestion by ultrasonic disintegration, Water. Sci. Technol. 42 (2000) 73–80, https://doi.org/10.2166/wst.2000.0174.
[4] J. Gostiša, B. Bizjan, Ž. Pandur, M. Levstek, B. Širok, M. Zupanc, Sludge bulking control using a hydrodynamic cavitation generator, in: Japan Society of Sonochemistry (Ed.), ESS-JSS-AOSS Joint Sonochemistry Conference, Japan Society of Sonochemistry, Online, 2021.
[5] I. Lee, J.-I. Han, The effects of waste-activated sludge pretreatment using hydrodynamic cavitation for methane production, Ultrason. Sonochem 20 (2013) 1450–1455, https://doi.org/10.1016/j.ultsonch.2013.03.006.
[6] M. Petkovšek, M. Mlakar, M. Levstek, M. Stražar, B. Širok, M. Dular, A novel rotation generator of hydrodynamic cavitation for waste-activated sludge disintegration, Ultrason. Sonochem 26 (2015) 408–414, https://doi.org/10.1016/j.ultsonch.2015.01.006.
[7] J. Vilarroig, R. Martínez, E. Zuriaga-Agustí, S. Torró, M. Galián, S. Chiva, Design and optimization of a semi-industrial cavitation device for a pretreatment of an anaerobic digestion treatment of excess sludge and pig slurry, Water. Environ. Res 92 (2020) 2060–2071, https://doi.org/10.1002/wer.1366.
[8] M. Zupanc, B.B. Humar, M. Dular, J. Gostiša, M. Hočevar, S.K. Repinc, M. Krzyk, L. Novak, J. Ortar, Ž. Pandur, B. Stres, M. Petkovšek, The use of hydrodynamic cavitation for waste-to-energy approach to enhance methane production from waste activated sludge, J. Environ. Manage 347 (2023) 119074, https://doi.org/10.1016/j.jenvman.2023.119074.
[9] M.S. Islam, V.V. Ranade, Enhancement of biomethane potential of brown sludge by pre-treatment using vortex based hydrodynamic cavitation, Heliyon 9 (2023) e18345, https://doi.org/10.1016/j.heliyon.2023.e18345.
[10] H. Son, S. Na, M. Guo, D.K. Le, X. Sun, J.Y. Yoon, Intermediate Treatment of Sewage Sludge Using an Advanced Rotational Hydrodynamic Cavitation Reactor for Improvement of Biogas Production, Available at SSRN: Https://Ssrn.Com/Abstract=4743090 or Http://Dx.Doi.Org/10.2139/Ssrn.4743090 (2024).
[11] M. Blagojevič, G. Rak, B. Bizjan, S. Kolbl Repinc, A review on rotary generators of hydrodynamic cavitation for wastewater treatment and enhancement of anaerobic digestion process, Processes 11 (2023) 514, https://doi.org/10.3390/pr11020514.
[12] S.J. De-Nasri, V.P. Sarvothaman, S. Nagarajan, P. Manesiotis, P.K.J. Robertson, V. V. Ranade, Quantifying OH radical generation in hydrodynamic cavitation via coumarin dosimetry: Influence of operating parameters and cavitation devices, Ultrason. Sonochem 90 (2022) 106207, https://doi.org/10.1016/j.ultsonch.2022.106207.
[13] Y. Hu, Z. Zhang, C. Yang, Measurement of hydroxyl radical production in ultrasonic aqueous solutions by a novel chemiluminescence method, Ultrason. Sonochem 15 (2008) 665–672, https://doi.org/10.1016/j.ultsonch.2008.01.001.
[14] M. Zupanc, M. Petkovšek, J. Zevnik, G. Kozmus, A. Šmid, M. Dular, Anomalies detected during hydrodynamic cavitation when using salicylic acid dosimetry to measure radical production, Chem. Eng. J. 396 (2020) 125389, https://doi.org/10.1016/j.cej.2020.125389.
[15] T.P. Wong, R.W. Babcock, T. Uekawa, J. Schneider, B. Hu, Effects of Waste Activated Sludge Extracellular Polymeric Substances on Biosorption, Water. (basel) 14 (2022) 218, https://doi.org/10.3390/w14020218.
[16] G. Zhen, X. Lu, Y. Li, Y. Zhao, B. Wang, Y. Song, X. Chai, D. Niu, X. Cao, Novel insights into enhanced dewaterability of waste activated sludge by Fe(II)-activated persulfate oxidation, Bioresour. Technol 119 (2012) 7–14, https://doi.org/10.1016/j.biortech.2012.05.115.
[17] S. Kolbl Repinc, B. Bizjan, V. Budhiraja, M. Dular, J. Gostiša, B. Brajer Humar, A. Kaurin, A. Kržan, M. Levstek, J.F.M. Arteaga, M. Petkovšek, G. Rak, B. Stres, B. Širok, E. Žagar, M. Zupanc, Integral analysis of hydrodynamic cavitation effects on waste activated sludge characteristics, potentially toxic metals, microorganisms and identification of microplastics, Science of The Total Environment 806 (2022) 151414. 10.1016/j.scitotenv.2021.151414.
[18] T.T.H. Pham, S.K. Brar, R.D. Tyagi, R.Y. Surampalli, Influence of ultrasonication and Fenton oxidation pre-treatment on rheological characteristics of wastewater sludge, Ultrason. Sonochem 17 (2010) 38–45, https://doi.org/10.1016/j.ultsonch.2009.06.007.
[19] T.T.H. Pham, S.K. Brar, R.D. Tyagi, R.Y. Surampalli, Ultrasonication of wastewater sludge—Consequences on biodegradability and flowability, J. Hazard. Mater 163 (2009) 891–898, https://doi.org/10.1016/j.jhazmat.2008.07.091.
[20] M. Ruiz-Hernando, J. Labanda, J. Llorens, Effect of ultrasonic waves on the rheological features of secondary sludge, Biochem. Eng. J 52 (2010) 131–136, https://doi.org/10.1016/j.bej.2010.07.012.
[21] M. Ruiz-Hernando, F.-X. Simón, J. Labanda, J. Llorens, Effect of ultrasound, thermal and alkali treatments on the rheological profile and water distribution of waste activated sludge, Chem. Eng. J. 255 (2014) 14–22, https://doi.org/10.1016/j.cej.2014.06.036.
[22] D.P. Mohapatra, S.K. Brar, R.D. Tyagi, P. Picard, R.Y. Surampalli, Ferro-sonication and partial ozonation pre-treatment and biotransformation of wastewater sludge for degradation of bisphenol A: Rheology studies, Chem. Eng. Sci 81 (2012) 20–27, https://doi.org/10.1016/j.ces.2012.06.054.
[23] J. Walczak, A. Dzido, H. Jankowska, P. Krawczyk, M. Zubrowska-Sudol, Effects of various rotational speeds of hydrodynamic disintegrator on carbon, nutrient, and energy recovery from sewage sludge, Water. Res 243 (2023) 120365, https://doi.org/10.1016/j.watres.2023.120365.
[24] M. Blagojevič, B. Bizjan, M. Zupanc, J. Gostiša, L.S. Perše, U.G. Centa, B. Stres, U. Novak, B. Likozar, G. Rak, S.K. Repinc, Preliminary analysis: Effect of a rotary generator of hydrodynamic cavitation on rheology and methane yield of wastewater sludge, Ultrason. Sonochem (2024) 106943, https://doi.org/10.1016/j.ultsonch.2024.106943.
[25] Ž. Pandur, J. Zevnik, D. Podbevšek, B. Stojković, D. Stopar, M. Dular, Water treatment by cavitation: Understanding it at a single bubble - bacterial cell level, Water. Res 236 (2023) 119956, https://doi.org/10.1016/j.watres.2023.119956.
[26] A.V. Mohod, A.C.S.C. Teixeira, M.V. Bagal, P.R. Gogate, R. Giudici, Degradation of organic pollutants from wastewater using hydrodynamic cavitation: A review, J. Environ. Chem. Eng 11 (2023) 109773, https://doi.org/10.1016/j.jece.2023.109773.
[27] J. Gostiša, P. Drešar, M. Hočevar, M. Dular, Computational analysis of flow conditions in hydrodynamic cavitation generator for water treatment processes, Can. J. Chem. Eng 100 (2022) 3502–3516, https://doi.org/10.1002/cjce.24572.
[28] J. Gostiša, B. Širok, B. Bizjan, J. Ortar, M. Dular, M. Zupanc, Multiparametric experimental analysis of the pin disc rotational cavitation generator, Eng. Sci. Technol,. Int. J. 38 (2023) 101323, https://doi.org/10.1016/j.jestch.2022.101323.
[29] N. Eshtiaghi, F. Markis, S.D. Yap, J.-C. Baudez, P. Slatter, Rheological characterisation of municipal sludge: A review, Water. Res 47 (2013) 5493–5510, https://doi.org/10.1016/j.watres.2013.07.001.
[30] VOKA SNAGA, Centralna čistilna naprava Ljubljana Tehnološki podatki, Https://Www.Vokasnaga.Si/ (2024). https://www.vokasnaga.si/o-druzbi/centralna-cistilna-naprava-ljubljana/tehnoloski-podatki (accessed September 9, 2024).
[31] APHA, Standard Methods for the Examination of Water and Wastewater, 23rd ed., Washington DC: American Public Health Association., 2017.
[32] J. Gostiša, B. Širok, S. Kolbl Repinc, M. Levstek, M. Stražar, B. Bizjan, M. Zupanc, Performance evaluation of a novel pilot-scale pinned disc rotating generator of

hydrodynamic cavitation, Ultrason. Sonochem 72 (2021) 105431, https://doi.org/10.1016/j.ultsonch.2020.105431.
[33] J.R. Helms, A. Stubbins, J.D. Ritchie, E.C. Minor, D.J. Kieber, K. Mopper, Absorption spectral slopes and slope ratios as indicators of molecular weight, source, and photobleaching of chromophoric dissolved organic matter, Limnol. Oceanogr 53 (2008) 955–969, https://doi.org/10.4319/lo.2008.53.3.0955.
[34] B. Vidmar, A. Oberlintner, B. Stres, B. Likozar, U. Novak, Biodegradation of polysaccharide-based biocomposites with acetylated cellulose nanocrystals, alginate and chitosan in aqueous environment, Int. J. Biol. Macromol 252 (2023) 126433, https://doi.org/10.1016/j.ijbiomac.2023.126433.
[35] W.-H. Liu, H. Zhang, P. Sun, Y.-P. Zeng, Y.-Y. Gao, H.-F. Wang, R.J. Zeng, Yield stress Measurement of municipal sludge: A comprehensive evaluation of testing methods and concentration effects using a rotational rheometer, Environ. Res 250 (2024) 118554, https://doi.org/10.1016/j.envres.2024.118554.
[36] Ø. Hammer, D.A.T. Harper, P.D. Ryan, PAST: Paleontological statistics software package for education and data analysis, Palaeontologia Electronica 4(1): 9pp (2001). http://palaeo-electronica.org/2001_1/past/issue1_01.htm (accessed November 13, 2023).
[37] Øyvind Hammer, PAST PAleontological STatistics Version 5.0 Reference manual, Natural History Museum University of Oslo (2024). https://www.nhm.uio.no/english/research/resources/past/downloads/past5manual.pdf (accessed January 15, 2025).
[38] Y. Lv, K. Xiao, J. Yang, Y. Zhu, K. Pei, W. Yu, S. Tao, H. Wang, S. Liang, H. Hou, B. Liu, J. Hu, Correlation between oxidation-reduction potential values and sludge dewaterability during pre-oxidation, Water. Res 155 (2019) 96–105, https://doi.org/10.1016/j.watres.2019.02.049.
[39] H. Kim, B. Koo, X. Sun, J.Y. Yoon, Investigation of sludge disintegration using rotor-stator type hydrodynamic cavitation reactor, Sep. Purif. Technol 240 (2020) 116636, https://doi.org/10.1016/j.seppur.2020.116636.
[40] H. Kim, X. Sun, B. Koo, J.Y. Yoon, Experimental Investigation of Sludge Treatment Using a Rotor-Stator Type Hydrodynamic Cavitation Reactor and an Ultrasonic Bath, Processes 7 (2019) 790, https://doi.org/10.3390/pr7110790.
[41] M. Zubrowska-Sudol, A. Dzido, A. Garlicka, P. Krawczyk, M. Stępień, K. Umiejewska, J. Walczak, M. Wołowicz, K. Sytek-Szmeichel, Innovative Hydrodynamic Disintegrator Adjusted to Agricultural Substrates Pre-treatment Aimed at Methane Production Intensification—CFD Modelling and Batch Tests, Energies. (basel) 13 (2020) 4256, https://doi.org/10.3390/en13164256.
[42] U. Schmitz, Protein analysis as a simple method for the quantitative assessment of sewage sludge disintegration, Water. Res 34 (2000) 3682–3685, https://doi.org/10.1016/S0043-1354(00)00091-9.
[43] A. Dzido, J. Walczak, H. Jankowska, P. Krawczyk, E.G. Özbayram, M. Żubrowska-Sudoł, Hydrodynamic disintegration effects assessment by CFD modelling integrated with bench tests, J. Environ. Manage 367 (2024), https://doi.org/10.1016/j.jenvman.2024.121948.
[44] I. Zawieja, M. Worwag, K. Brzeska, Methane fermentation of the excess sludge sonicated and oxidized with Fenton's reagent, Desalination, Water. Treat 232 (2021) 216–224, https://doi.org/10.5004/dwt.2021.27322.
[45] T. Lippert, J. Bandelin, F. Schlederer, J.E. Drewes, K. Koch, Effects of ultrasonic reactor design on sewage sludge disintegration, Ultrason. Sonochem 68 (2020), https://doi.org/10.1016/j.ultsonch.2020.105223.
[46] M. Tytła, K. Widziewicz-Rzońca, J. Kernert, Z. Bernaś, K. Słaby, First Comprehensive Analysis of Potential Ecological Risk and Factors Influencing Heavy Metals Binding in Sewage Sludge from WWTPs Using the Ultrasonic Disintegration Process, Water. (switzerland) 15 (2023), https://doi.org/10.3390/w15040666.
[47] G. Erden, A. Filibeli, Ultrasonic pre-treatment of biological sludge: Consequences for disintegration, anaerobic biodegradability, and filterability, J. Chem. Technol. Biotechnol. 85 (2010) 145–150, https://doi.org/10.1002/jctb.2298.
[48] M.R. Carter, E.G. Gregorich, Soil Sampling and Methods of Analysis, CRC. Press (2007), https://doi.org/10.1201/9781420005271.
[49] R. Zeng, C.M. Mannaerts, C. Lievens, Assessment of UV-VIS spectra analysis methods for quantifying the absorption properties of chromophoric dissolved organic matter (CDOM), Front. Environ. Sci 11 (2023), https://doi.org/10.3389/fenvs.2023.1152536.
[50] A.M. Hansen, T.E.C. Kraus, B.A. Pellerin, J.A. Fleck, B.D. Downing, B. A. Bergamaschi, Optical properties of dissolved organic matter (DOM): Effects of biological and photolytic degradation, Limnol. Oceanogr 61 (2016) 1015–1032, https://doi.org/10.1002/lno.10270.
[51] F. Zhang, W. Zhang, S. Wu, X. Fu, S. Li, S. Yue, Analysis of UV–Vis spectral characteristics and content estimation of soil DOM under mulching practices, Ecol. Indic 138 (2022) 108869, https://doi.org/10.1016/j.ecolind.2022.108869.
[52] PROMEGA Application note, How do I determine the concentration, yield and purity of a DNA sample?, Https://Worldwide.Promega.Com/Resources/Pubhub/Enotes/How-Do-i-Determine-the-Concentration-Yield-and-Purity-of-a-Dna-Sample/ (2024).
[53] Q. Yu, X. Jin, Y. Zhang, Sequential pretreatment for cell disintegration of municipal sludge in a neutral Bio-electro-Fenton system, Water. Res 135 (2018) 44–56, https://doi.org/10.1016/j.watres.2018.02.012.
[54] P. Wiercik, M. Kuśnierz, M. Kabsch-Korbutowicz, A. Plucińska, P. Chrobot, Evaluation of changes in activated sludge and sewage sludge quality by FTIR analysis and laser diffraction, Desalination, Water. Treat 273 (2022) 114–125, https://doi.org/10.5004/dwt.2022.28855.
[55] S. Ruan, J. Deng, A. Cai, S. Chen, Y. Cheng, J. Li, Q. Li, X. Li, Improving dewaterability of waste activated sludge by thermally-activated persulfate oxidation at mild temperature, J. Environ. Manage 281 (2021) 111899, https://doi.org/10.1016/j.jenvman.2020.111899.
[56] J. Chen, J. Li, X. Zhang, Z. Wu, Pretreatments for enhancing sewage sludge reduction and reuse in lipid production, Biotechnol. Biofuels 13 (2020) 204, https://doi.org/10.1186/s13068-020-01844-3.
[57] B. Yang, Q. Pan, Q. Liu, X. Pan, Damage mechanisms of sludge flocs and cell structures by different pretreatment methods, Environ. Technol. Innov 30 (2023) 103134, https://doi.org/10.1016/j.eti.2023.103134.
[58] S.S. Arya, P.R. More, M.R. Ladole, K. Pegu, A.B. Pandit, Non-thermal, energy efficient hydrodynamic cavitation for food processing, process intensification and extraction of natural bioactives: A review, Ultrason. Sonochem 98 (2023) 106504, https://doi.org/10.1016/j.ultsonch.2023.106504.
[59] J.A. von Fraunhofer, Adhesion and Cohesion, Int. J. Dent 2012 (2012) 1–8, https://doi.org/10.1155/2012/951324.
[60] N.F. Gray, Capillary Suction Time (CST), in: Progress in Filtration and Separation, Elsevier, 2015: pp. 659–670. 10.1016/B978-0-12-384746-1.00017-3.
[61] J. Hou, C. Hong, W. Ling, J. Hu, W. Feng, Y. Xing, Y. Wang, C. Zhao, L. Feng, Research progress in improving sludge dewaterability: sludge characteristics, chemical conditioning and influencing factors, J. Environ. Manage 351 (2024) 119863, https://doi.org/10.1016/j.jenvman.2023.119863.
[62] T. Xiao, X. Dai, X. Wang, S. Chen, B. Dong, Enhanced sludge dewaterability via ozonation catalyzed by sludge derived biochar loaded with MnFe2O4: Performance and mechanism investigation, J. Clean. Prod 323 (2021) 129182, https://doi.org/10.1016/j.jclepro.2021.129182.
[63] T. Li, J. Yang, Y. Zhou, Y. Luo, B. Zhou, D. Fang, J. Li, L. Zhou, Enhancing sludge dewatering efficiency through bioleaching facilitated by increasing reactive oxygen species, Water. Res 231 (2023) 119622, https://doi.org/10.1016/j.watres.2023.119622.
[64] Y. Qi, J. Chen, H. Xu, S. Wu, Z. Yang, A. Zhou, Y. Hao, Optimizing sludge dewatering efficiency with ultrasonic Treatment: Insights into Parameters, Effects, and microstructural changes, Ultrason. Sonochem 102 (2024) 106736, https://doi.org/10.1016/j.ultsonch.2023.106736.
[65] D.-Q. He, Y.-J. Zhang, C.-S. He, H.-Q. Yu, Changing profiles of bound water content and distribution in the activated sludge treatment by NaCl addition and pH modification, Chemosphere 186 (2017) 702–708, https://doi.org/10.1016/j.chemosphere.2017.08.045.
[66] A.F. Santos, A.G.M. Ferreira, M.J. Quina, Efficient Management of Sewage Sludge from Urban Wastewaters with the Addition of Inorganic Waste: Focus on Rheological Properties, Clean. Technol. 4 (2022) 841–853, https://doi.org/10.3390/cleantechnol4030052.
[67] X. Su, Y. Tian, H. Li, C. Wang, New insights into membrane fouling based on characterization of cake sludge and bulk sludge: An especial attention to sludge aggregation, Bioresour. Technol 128 (2013) 586–592, https://doi.org/10.1016/j.biortech.2012.11.005.
[68] S. Al-Dawery, Effects of suspended solid and polyelectrolyte on settling and rheological properties of municipal activated sludge, J. Environ. Chem. Eng 4 (2016) 4731–4743, https://doi.org/10.1016/j.jece.2016.11.009.
[69] J. Liu, R. Wang, F. Gao, J. Zhou, K. Cen, Rheology and thixotropic properties of slurry fuel prepared using municipal wastewater sludge and coal, Chem. Eng. Sci 76 (2012) 1–8, https://doi.org/10.1016/j.ces.2012.04.010.
[70] Y. Mu, H.-Q. Yu, Rheological and fractal characteristics of granular sludge in an upflow anaerobic reactor, Water. Res 40 (2006) 3596–3602, https://doi.org/10.1016/j.watres.2006.05.041.
[71] B. Waltham, B. Örmeci, Fluorescence intensity, conductivity, and UV–vis absorbance as surrogate parameters for real-time monitoring of anaerobic digestion of wastewater sludge, J. Water. Process. Eng. 37 (2020) 101395, https://doi.org/10.1016/j.jwpe.2020.101395.
[72] B. Murovec, S. Kolbl, B. Stres, Methane Yield Database: Online infrastructure and bioresource for methane yield data and related metadata, Bioresour. Technol 189 (2015), https://doi.org/10.1016/j.biortech.2015.04.021.